Supporting Information

Hexaaminobenzene Derived Two-Dimensional Polymer Supercapacitor with High Specific Capacitance and Energy Density

Vivek C. Wakchaure,[1,2] Alagar R. Kottaichamy,[3] Aakash D. Nidhankar,[1,2] Kayaramkodath C. Ranjeesh,[1,2] Mohammed A. Nazrulla,[4] Musthafa O. Thotiyl,[3] Sukumaran S. Babu[*,1,2]

[1]Organic Chemistry Division, National Chemical Laboratory (CSIR-NCL), Dr. Homi Bhabha Road, Pune-411 008, India
[2]Academy of Scientific and Innovative Research (AcSIR), Ghaziabad-201 002, India
[3]Indian Institute of Science Education and Research (IISER), Dr. Homi Bhabha Road, Pashan, Pune-411 008, India
[4]Solid State and Structural Chemistry Unit, Indian Institute of Science (IISc), Bangalore 560107, India.

E-mail: sb.sukumaran@ncl.res.in*

Contents

	Page No
Experimental	**S2-S4**
Synthesis and characterization	**S5-S21**
Electrochemical measurements	**S22-S35**
Tables	**S36-S38**
References	**S39**

Experimental

Materials

All chemicals, pyromellitic dianhydride (PmDA), phthalic anhydride (PA) was purchased from Sigma-Aldrich and were used after sublimation. 1, 3, 5- tribromobenzene (Alfa Asear), Oleum (20%), KNO_3, sodium metal (Spectrochem) were used as received. The solvents such as toluene, dimethyl sulfoxide (DMSO), methanol and acetone were purchased from Finar Ltd.

General

All the reactions were carried out in over-dried round bottom flasks under an argon atmosphere unless otherwise mentioned. The ^{1}H, ^{13}C NMR spectra were recorded on a Bruker-400 MHz NMR spectrometer. The solid-state ^{13}C NMR spectrum was recorded on a Bruker-300 MHz NMR spectrometer instrument. The chemical shift values for ^{1}H (TMS as internal standard) and ^{13}C NMR are recorded in $CDCl_3$. FT-IR spectra were recorded using Bruker Alpha FT-IR spectrometer and reported in the frequency of absorption (cm^{-1}). Transmission electron microscopy (TEM, FEI Tecnai G2 F20 XTWIN). The electrochemical experiments were carried out using Biologic (VMP 300) potentiostat. The scanning electron microscope images were obtained using FEI, QUANTA 200 3D SEM instrument operating at 10, 15 and 20 kV, using tungsten filament as electron source and before imaging, the samples were sputtered with gold by using SCD 040 Balzers Union sputtered. X-ray photoelectron spectroscopy (XPS) analyses were performed on a Thermo Fisher Scientific Instruments UK, Sr.No.-KAS2020 with an Aluminium Kα+. BET adsorption experiment (up to 1 bar) was performed on a Quantachrome Quadrasorb automatic volumetric instrument. The pore diameter was calculated by nonlocal density functional theory (NLDFT). High-resolution mass spectra (HR-MS) were recorded on a Thermo Scientific Q-Exactive, Accela 1250 pump. High-resolution images of **P1** are captured by a high-resolution transmitted electron microscope (JEOL JEM 2200FES). Powder X-ray diffraction (PXRD) patterns were recorded on Phillips PANalytical diffractometer for Cu Kα radiation (α = 1.5406 Å), with a scan speed of 1° min^{-1} and a step size of 0.02° in 2θ.

Computational methodology

Density functional theory (DFT) based calculations for **M1** and **P1** are performed by employing a hybrid B3LYP (Becke, three-parameter, Lee-Yang-Parr) exchange-correlation functional as implemented in using Gaussian 09 (Revision C.01) suite of packages.[1] Double zeta valence polarization (dg-DZVP) basis sets have been used for all the atoms in **M1** and **P1**, viz., H, C, N and O. Restricted Kohn-Sham formalism has been utilized for the ground state (GS) optimizations of all the structures (**M1** and **P1**). Default convergence criterion with Berny algorithm and extra quadratically convergent (XQC) self-consistent field (SCF) methods are used for all the GS geometry optimizations. Optimized geometries are confirmed as the local minima with all the positive vibrational frequencies from simulated/theoretical IR. Natural atomic orbital and natural bond orbital analysis (NBO) program of Gaussian NBO Version 3.1[2] is used for the electrostatic potential mapping (ESP). Pink and green contours of ESP represent the positive and negative field, generated from Gauss View and plotted with the contour value of 0.03/0.06 from VESTA. (contour value has been selected in such a way to bring correlation for all the systems under study. All the images were plotted from Gauss View 5.0 and VESTA 3.4.4.[3]

Calculations

The specific capacitance (C_{sp}) was calculated from CV curves measured at various scan rates using the following equations.[4,5]

$$C_{sp} = \frac{I * \int dv}{m * v * \Delta V} \quad \ldots\ldots \textbf{(1)}$$

Where,

C_{sp} is specific capacitance (F g^{-1}),

I is current (A),

m is mass of the active material (g),

ν is the scan rate (mV s^{-1})

ΔV is the potential window (V).

The C_{sp} from the GCD curve was calculated using equation **(2)**

$$C_{sp} = \frac{I * \Delta t}{m * \Delta V} \quad \ldots\ldots \textbf{(2)}$$

Where

C_{sp} is specific capacitance (F g^{-1})

I is applied current (A)

ΔV represents the potential window (V)

Δt signifies discharge time (s)

m is the mass of the active material (g)

The energy density and power density of the materials were obtained from the equations:[2]

$$E = C_{sp} * \frac{\Delta V^2}{7.2} \quad \text{..... (3)}$$

$$P = E * \frac{3600}{\Delta t} \quad \text{..... (4)}$$

Where

E is the energy density (in Wh kg^{-1})

P is the power density (in W kg^{-1})

Δt is the total discharge time (in s).

Synthesis and characterization

Synthesis of Benzene-1,2,3,4,5,6-hexaamine (HAB)

The synthesis of HAB has been conducted by using a reported procedures.[6,7]

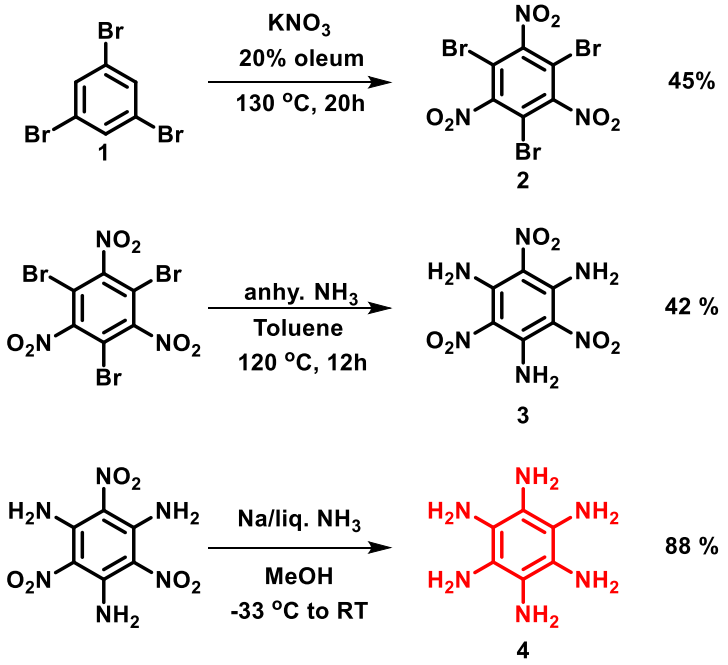

Scheme S1: Synthesis of benzene-1,2,3,4,5,6-hexaamine (HAB).

1,3,5-Tribromo-2,4,6-trinitrobenzene (2)

To a vigorously stirred solution of oleum (120 mL, 20%) at 0 °C, KNO_3 (34.69 g, 9 eq.) was added portion wisely. The resulting mixture was then heated to 110 °C, and 1,3,5-tribromobenzene (12 g, 1 eq.) was added slowly. The temperature was raised to 130-135 °C and continues heating for 18 h. After cooling to room temperature, the viscous mixture was poured to flaked ice. The solid which separated was collected, washed with water and dried. Recrystallization from chloroform provided the product as a pale yellow solid (7.7 g, 45%).

IR (KBR): 1539, 1338, 939, 828, 723, 544 cm^{-1}.

1,3,5-Triamino-2,4,6-trinitrobenzene (3)

Approximately 30 ml of anhydrous ammonia was condensed in the two necked round bottom flask. 1,3,5-tribromo-2,4,6-trinitrobenzene (1.00 gm) was dissolved in toluene (15 ml), add into the reaction mixture dropwise and allow to keep the reaction at -78 °C for about 1 h. Then keep the reaction mixture under reflux for 12 h. After cooling to room temperature, the

yellow solid was collected and washed with toluene and methanol to get a pure product as a yellow solid (242 mg, 42%).

IR (KBr): 3313, 3210, 1616, 1545, 1445, 1405, 1221, 1174, 697 cm^{-1}.

^{1}H NMR (400 MHz, D_2O): 7.19 (bs).

Solid-state carbon **^{13}C CP-MAS:** 151.56, 113.26.

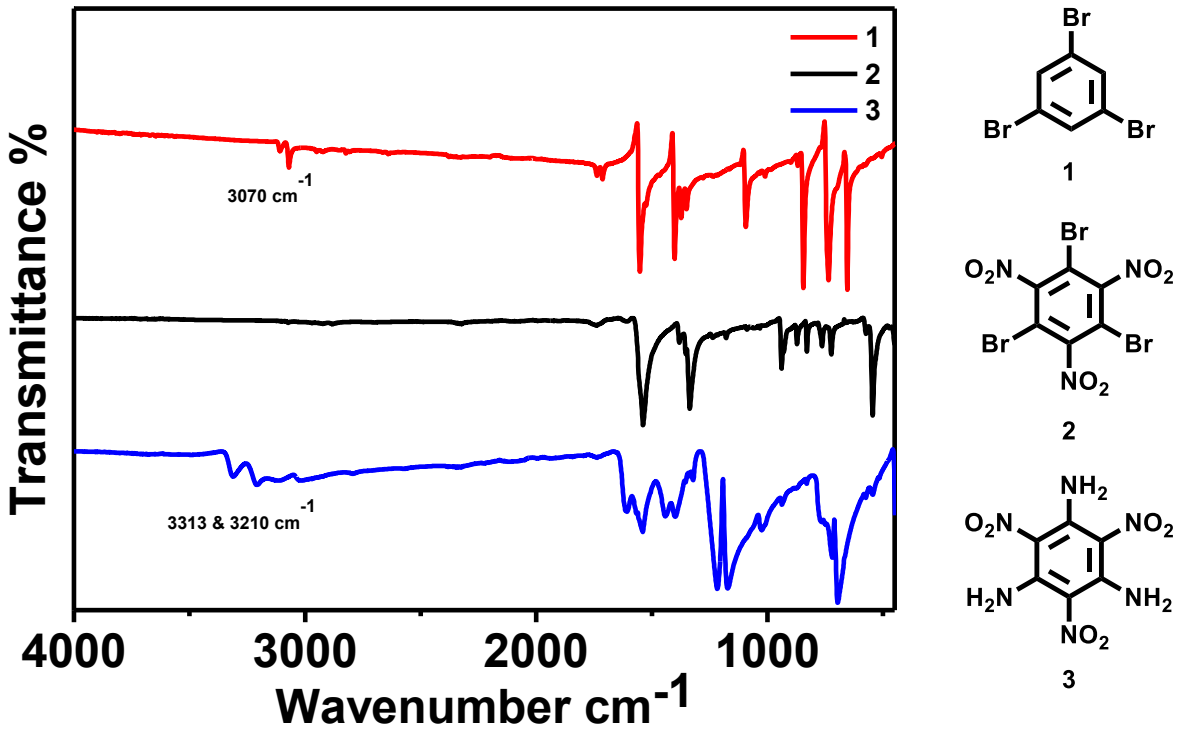

Figure S1: FTIR of compounds **1**, **2** and **3**.

*The Ar-CH starching frequency (3070 cm^{-1}) in compound **2** has been disappeared after nitration of **1**. Further reaction of **2** with ammonia yields **3** showing characteristic asymmetric & symmetric starching frequencies of amines at 3313 and 3210 cm^{-1}.*

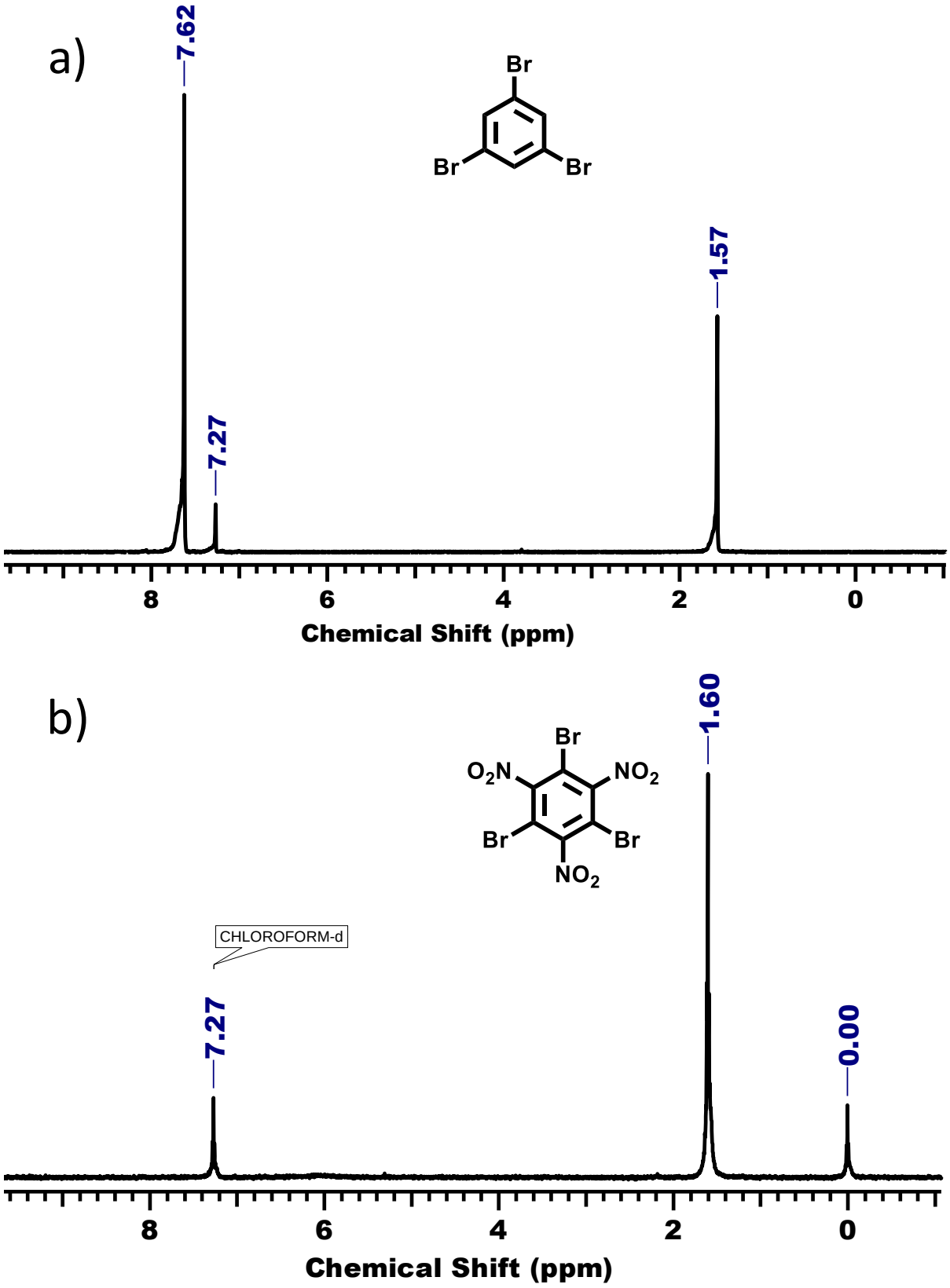

Figure S2: ^{1}H NMR spectra of a) **1** and b) **2**.

*^{1}H NMR of 1,3,5-tribromobenzene shows one singlet at 7.62 ppm for aromatic Ar-H, which has been disappeared after nitration (compound **2**).*

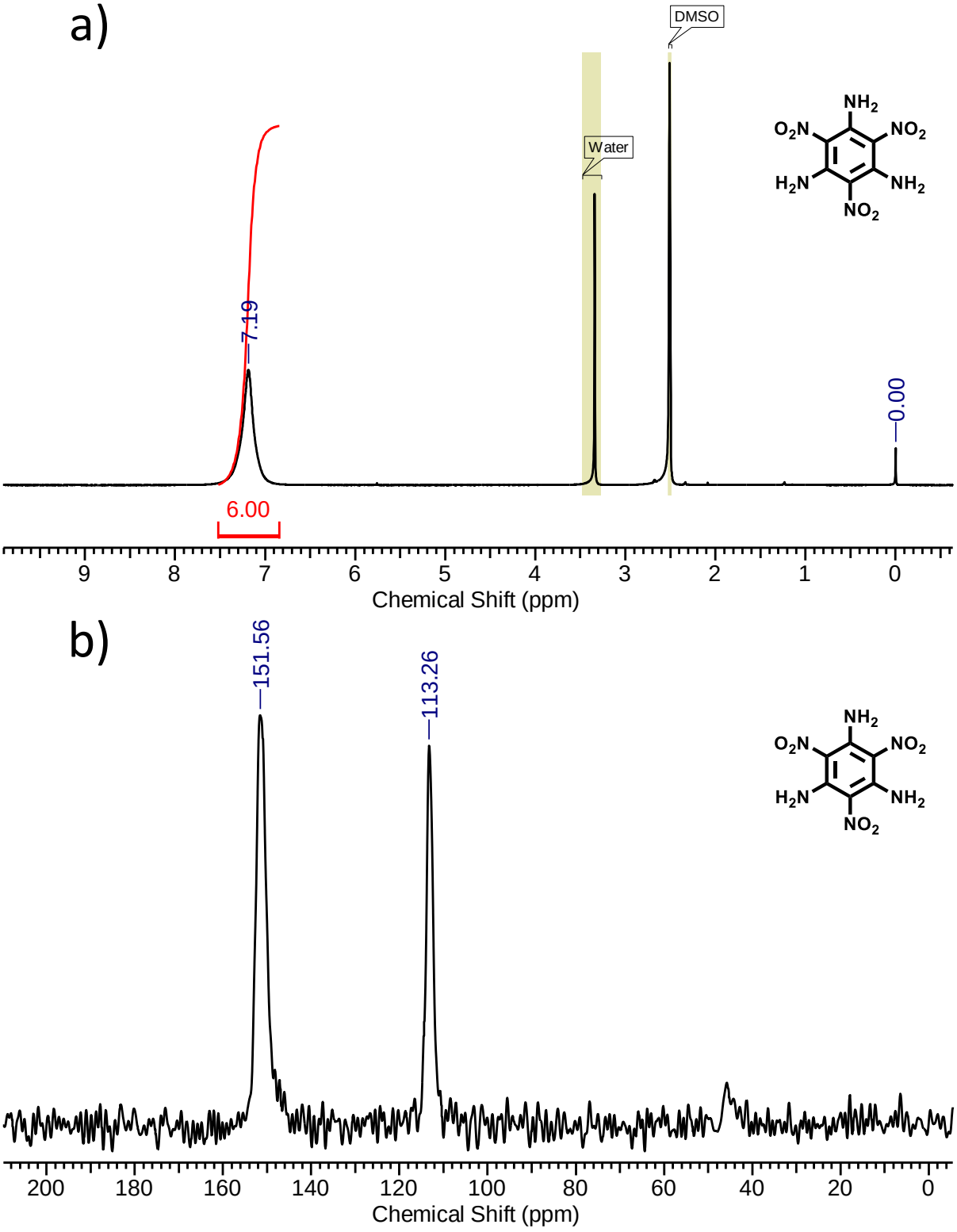

Figure S3: a) ^{1}H NMR and b) ^{13}C CP-MAS NMR spectra of **3** in DMSO-d_6.

*Compound **2** on further amination shows broad singlet for Ar-NH_2 proton at 7.19 ppm in DMSO-d_6. Since the solubility of **2** is less, the solid-state ^{13}C NMR spectrum was recorded, which shows two different carbon peaks.*

Hexaaminobenzene (HAB) (4)

A suspension of 310 mg 1,3,5-triamino-2,4,6-trinitrobenzene in 10 ml degassed methanol was stirred in a 100 mL 3-neck round-bottom flask equipped with a gas condenser and a gas exit valve. The suspension was cooled to -33 ^{o}C and approximately 10 ml of anhydrous ammonia was allowed to condense in the reaction mixture. 500 mg of sodium was then added to the reaction mixture in very small portions. The rate of addition of sodium was controlled to maintain the slow reflux of ammonia in the reaction mixture. A transient blue color was observed with the addition of sodium. Once the addition of sodium was complete, the reaction was allowed to stir for another 30 min. During this time the blue color of the reaction mixture was slowly discharged. The gas exit valve was then opened and the reaction was then slowly warmed to room temperature to allow the excess ammonia to escape. A cream-colored precipitate was seen in the reaction mixture which was then vacuum-filtered under argon. It was washed first with degassed ethanol followed by degassed diethyl ether to give HAB as a cream-colored solid.

FTIR (cm^{-1}): 3317, 3209, 1607, 1613.2, 1539, 1220, 1173.

^{1}H NMR (400 MHz, D_2O): 3.3 (s).

^{13}C NMR (100 MHz, D_2O): 119.07.

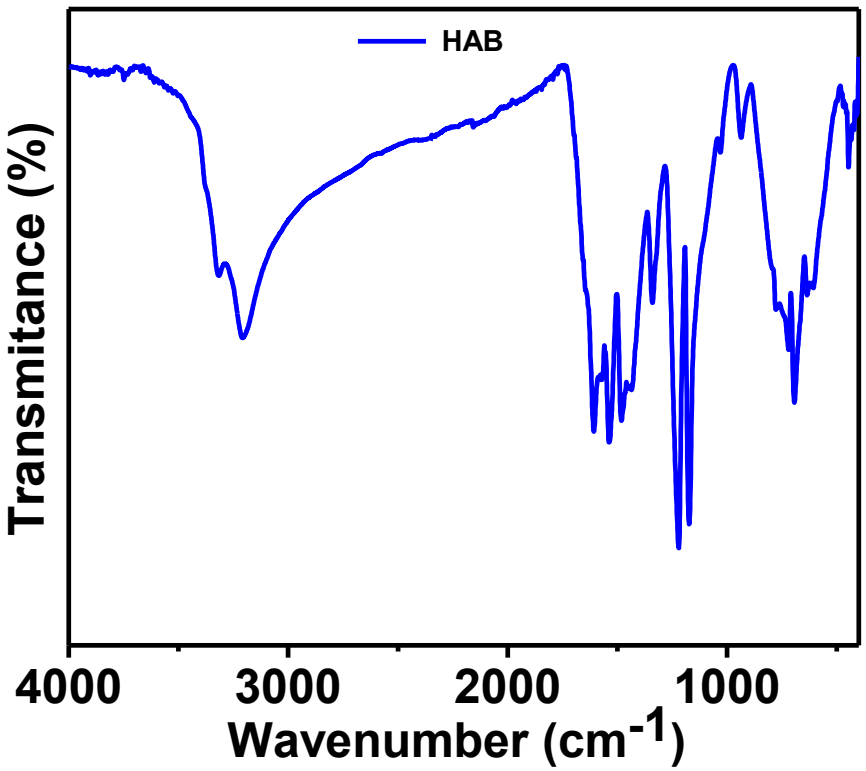

Figure S4: FTIR of hexaaminobenzene (**HAB**).

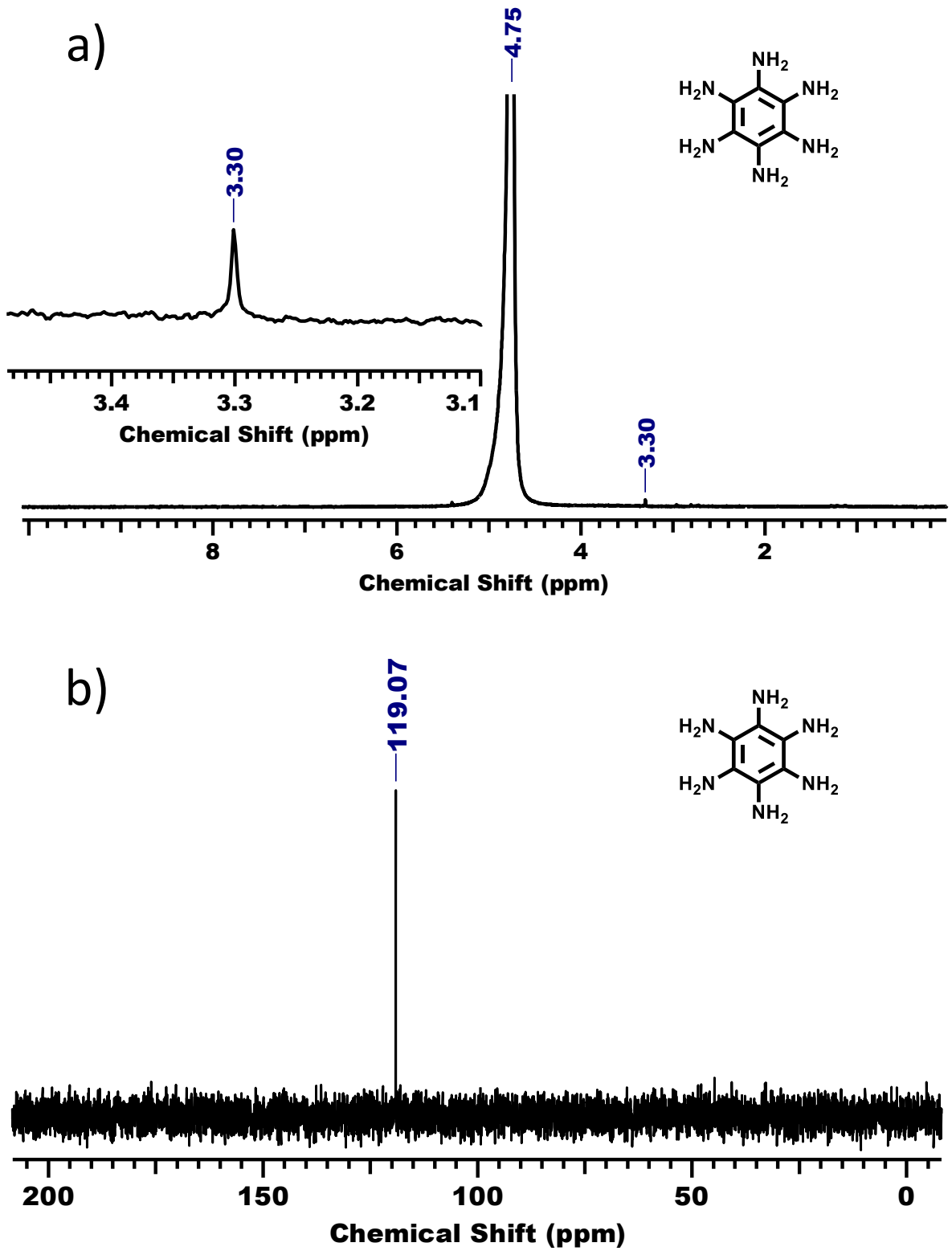

Figure S5: a) ^{1}H NMR and b) ^{13}C NMR spectra of **HAB** in D_2O.

The prepared HAB has sufficient purity and found that it is very much unstable, hence used immediately after filtration under argon for the next reactions.

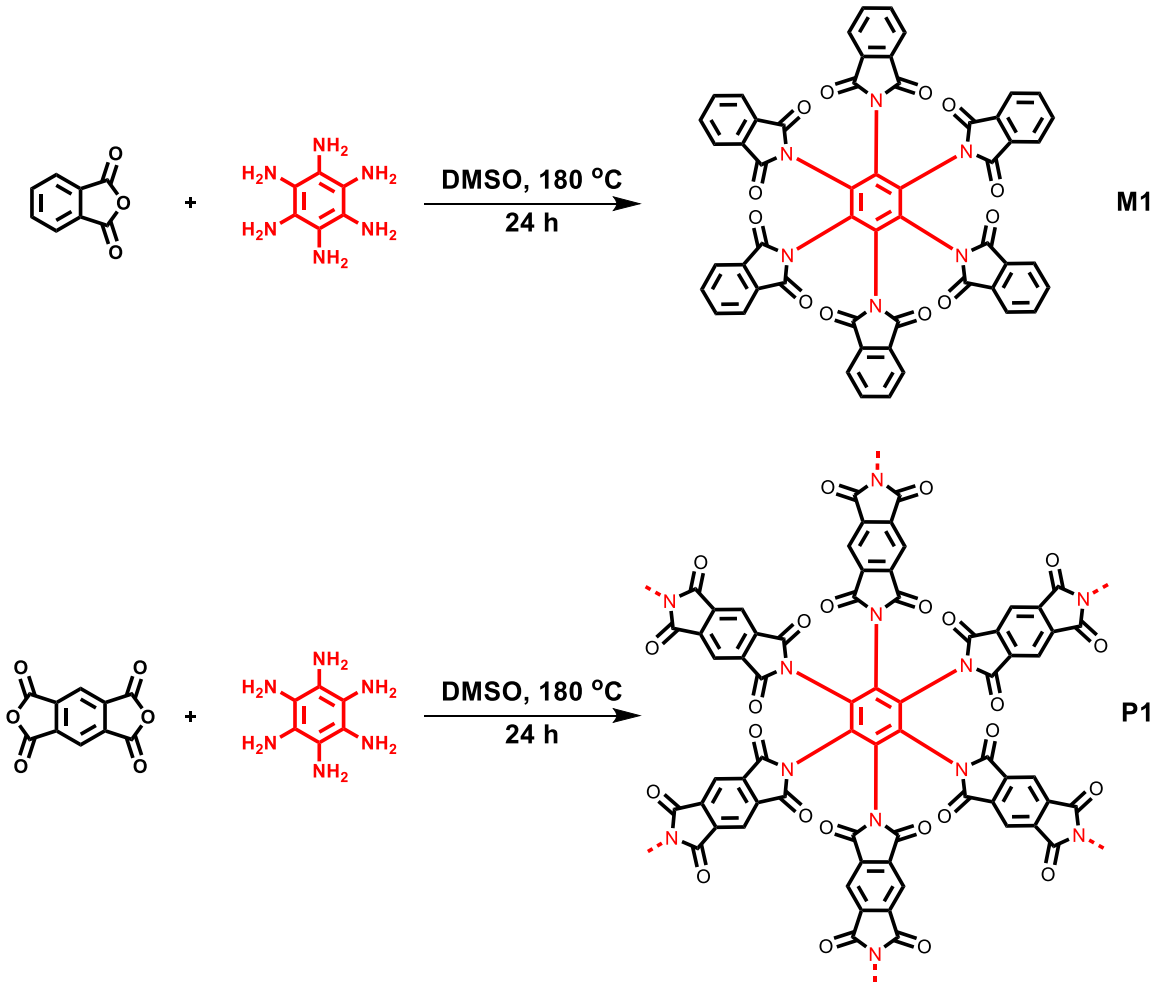

Scheme S2: Synthetic scheme of monomer **M1** and polymer **P1**.

Monomer **M2** has been synthesized by using a reported procedure.[8]

Characterization

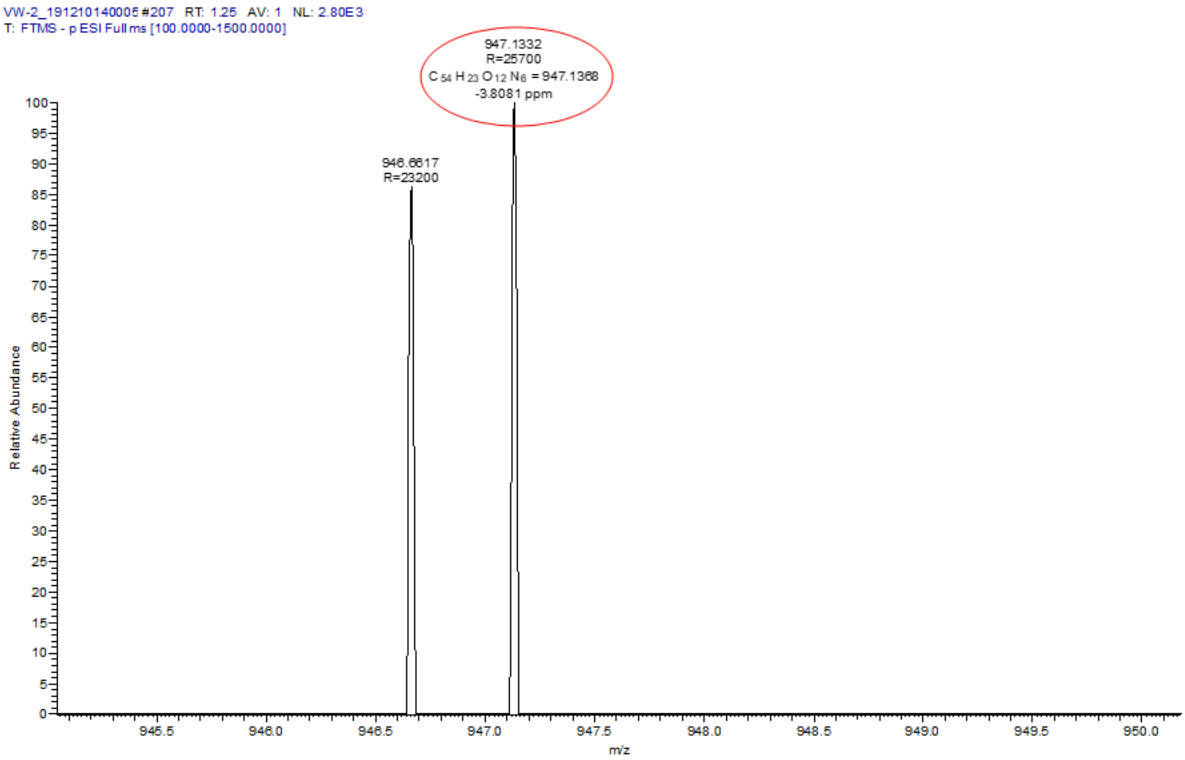

Figure S6: HRMS of **M1**.

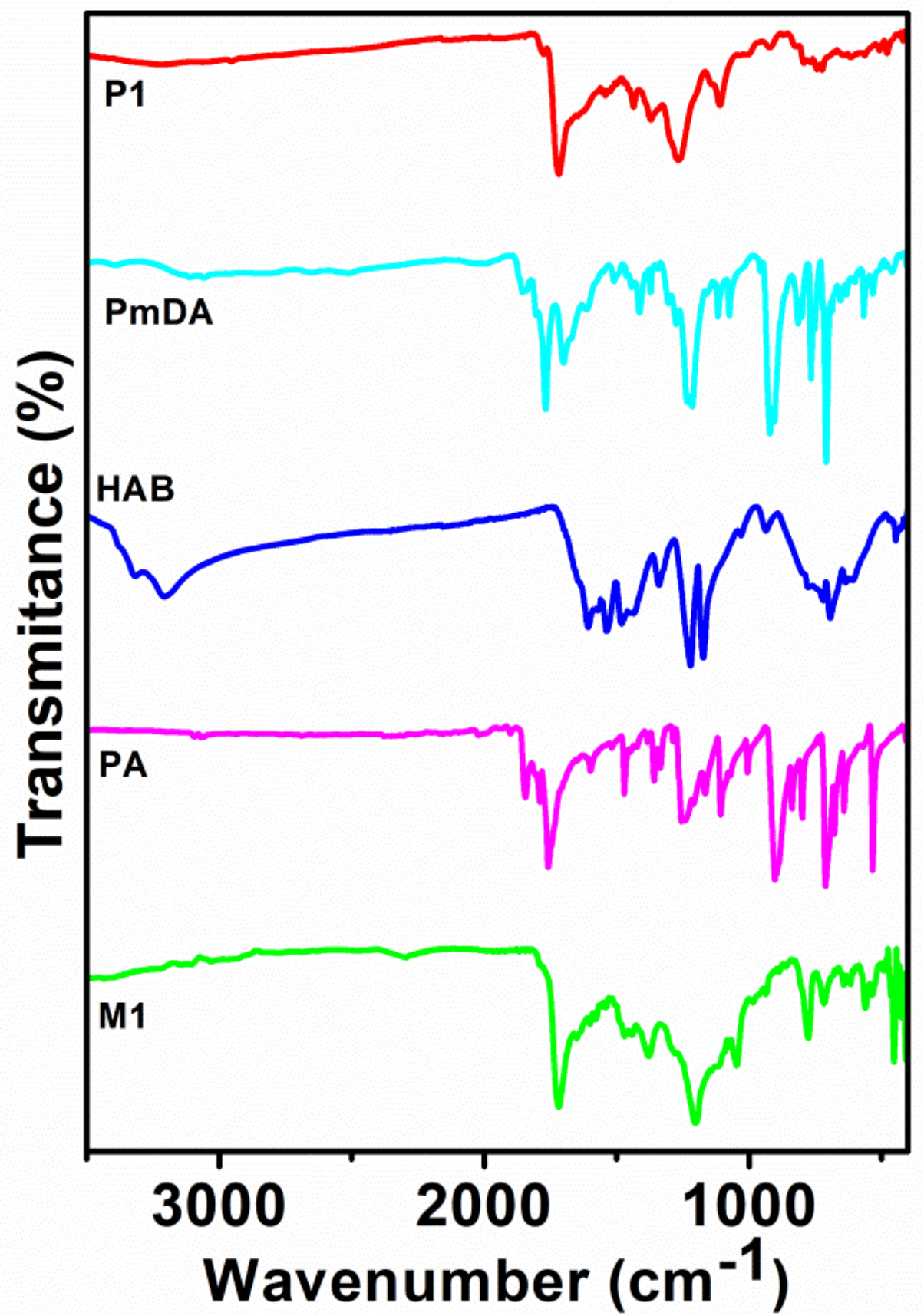

Figure S7: FT-IR spectra of starting materials, **M1** and **P1**.

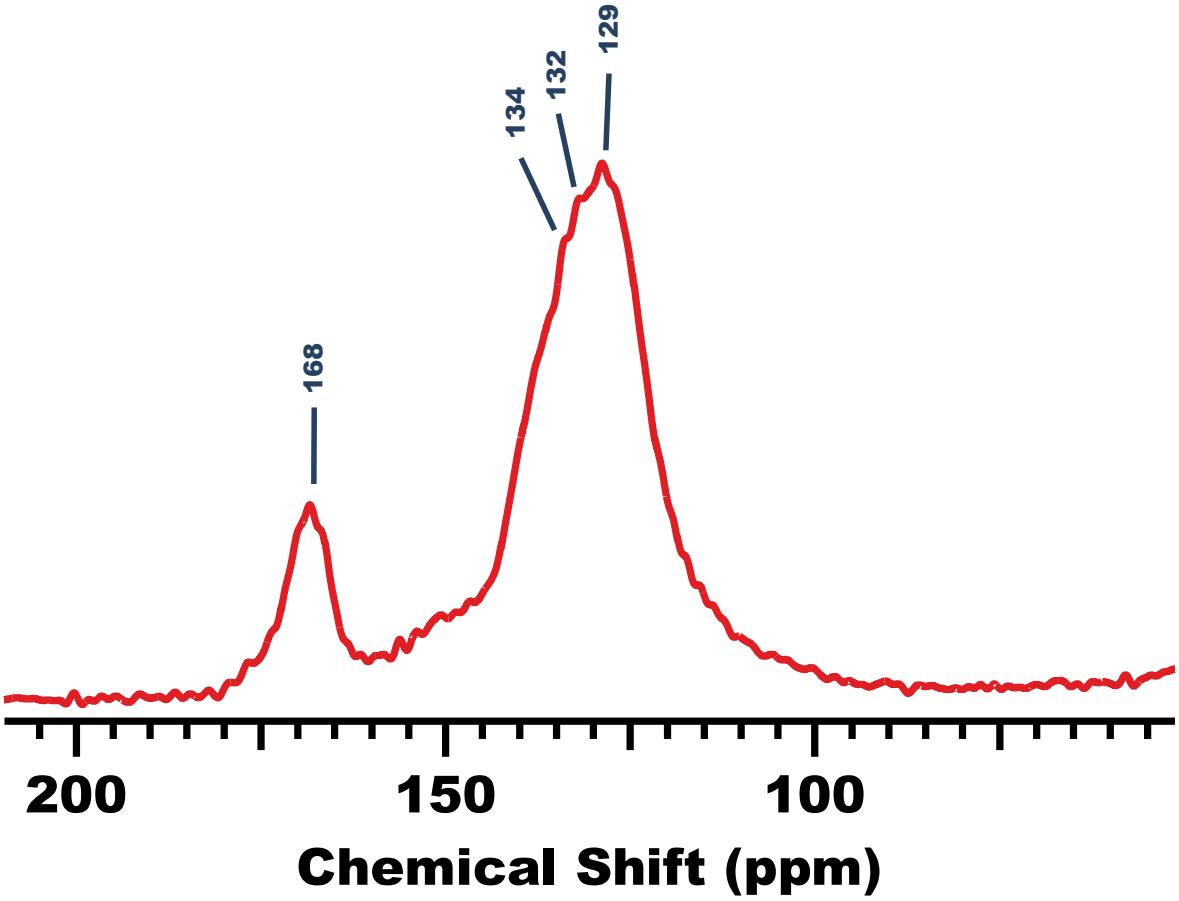

Figure S8: Solid-state ^{13}C NMR of **P1**.

P1 *shows broad solid-state* ^{13}*C NMR spectrum having peaks located at 168 ppm (imide carbonyls) and 129,132,134 ppm (aromatic carbon). Which was comparible with reported 3D-porous crystalline polyimide covalent organic framework (J. Am. Chem. Soc.* ***2015****, 137, 8352). This 3D-COF is synthesized by using 1,3,5,7-tetraaminoadamantane and pyromellitic dianhydride (****PI-COF-4****). The synthesized polymer* ***PI-COF-4*** *shows FT-IR peak for a carbonyl (C=O, 1774 and 1778 cm*$^{-1}$*) and for nitrogen (C-N-C, 1336 cm*$^{-1}$*), which are in correlation with the FTIR spectra of* ***P1****. Similarly,* ***P1-COF-4*** *shows a broad* ^{13}*C NMR spectra with 165 ppm (imide carbonyls) and 119,125,131 ppm (aromatic carbon).*
We strongly believe that the broad peaks in solid-state ^{13}*C NMR spectra are due to the chemical shift anisotropy originating from the lack of ordered molecular packing in the solid-state.*

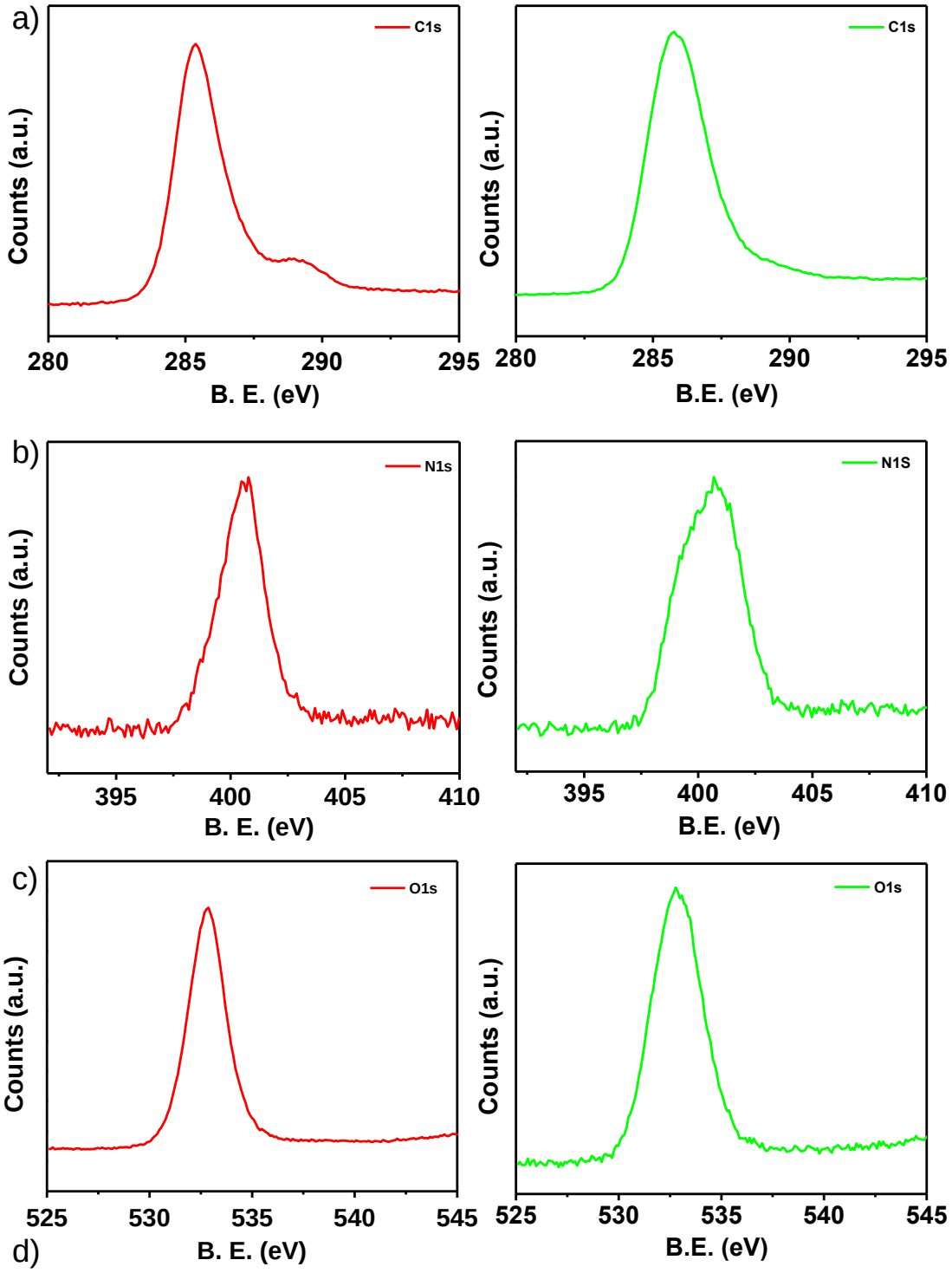

Name	Peak (BE)	Atomic %
N1s	401.12	8.52
C1s	286.83	73.84
O1s	533.39	12.24

Figure S9: XPS analysis showing profiles of a) $C_{1S,}$ b) N_{1S} and c) O_{1S} for **P1** (left) and **M1** (right). d) Table showing the atomic percentage of $C_{1S,}$ $N_{1S,}$ and O_{1S} of **M1**.

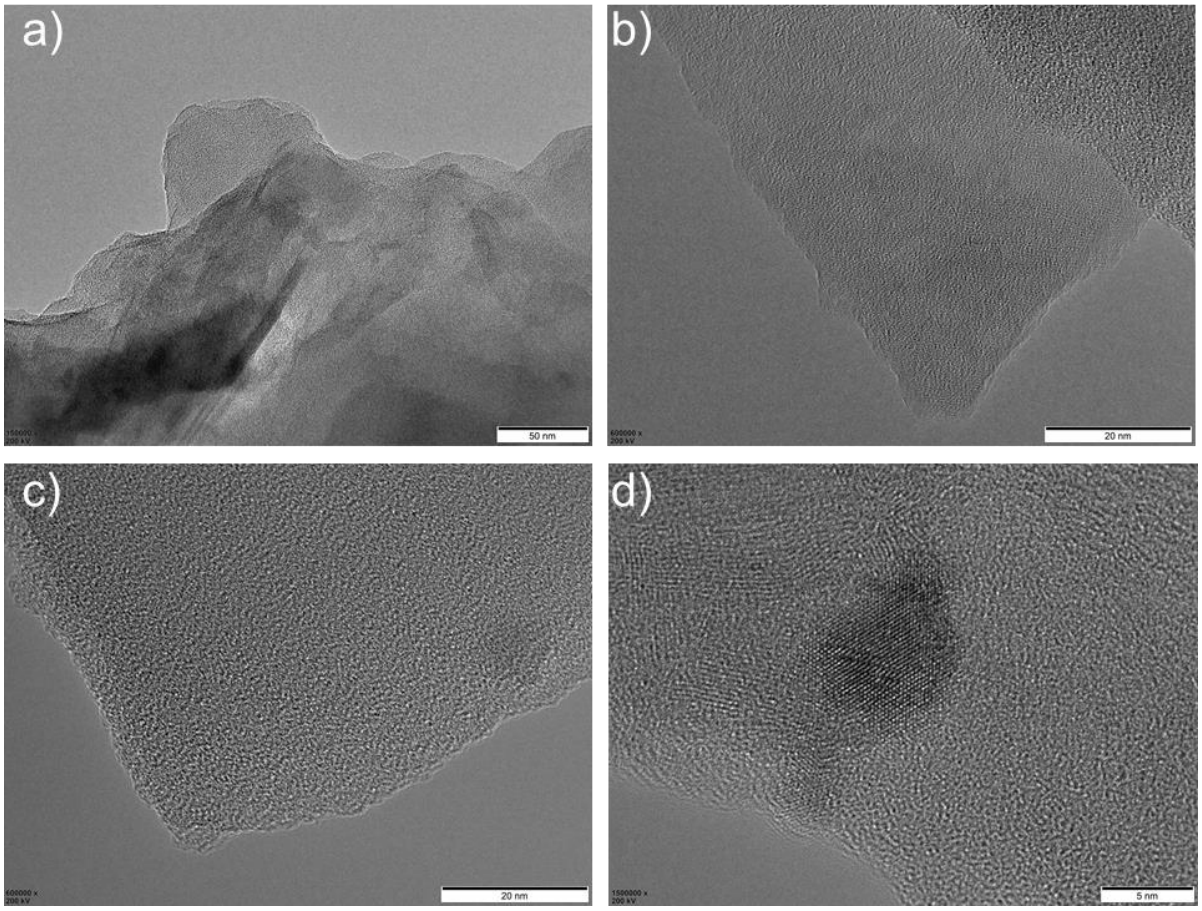

Figure S10: a-d) HR-TEM images of **P1**.

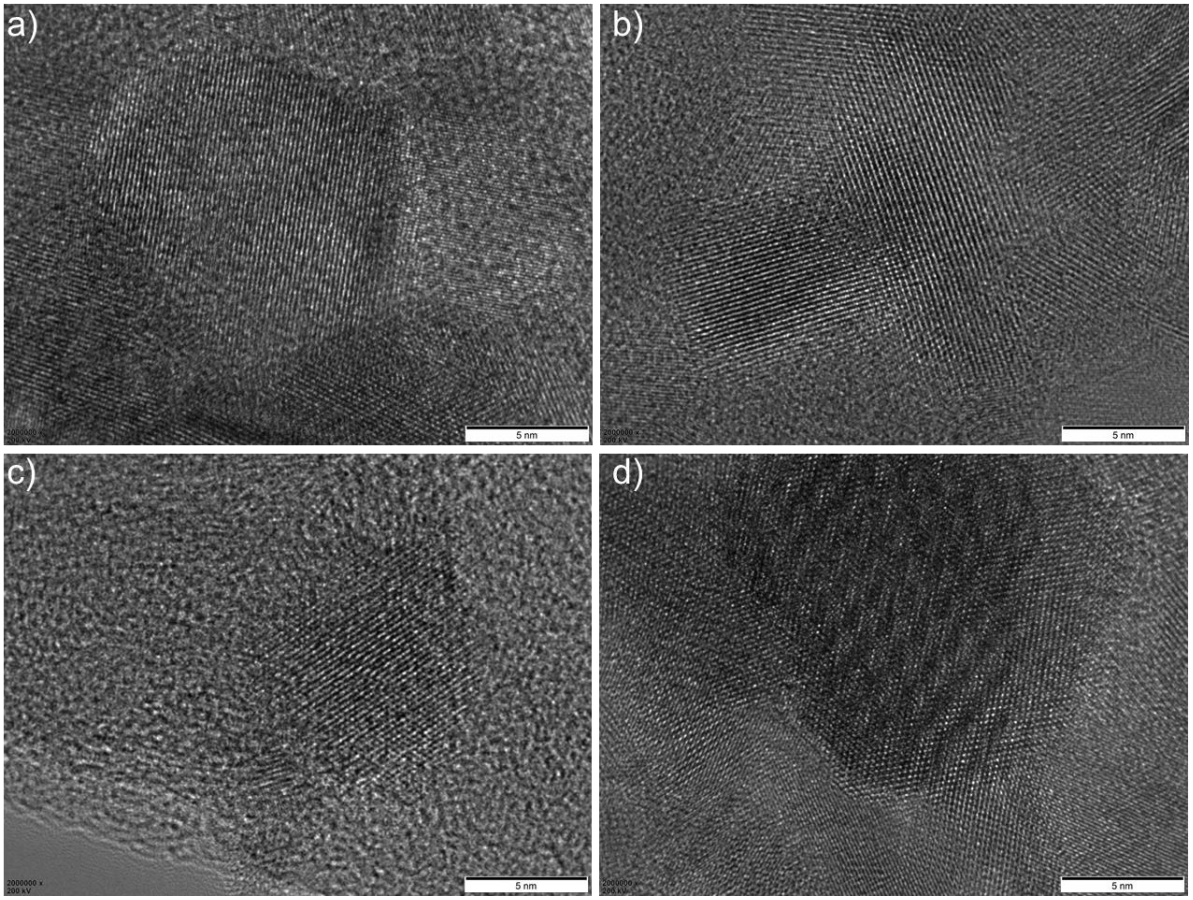

Figure S11: a-d) HR-TEM images of **P1**.

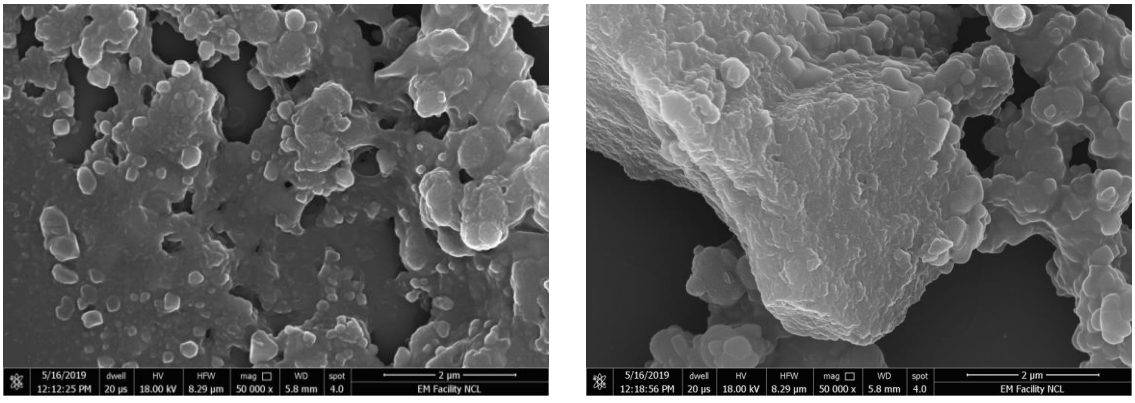

Figure S12: FE-SEM images of **P1**.

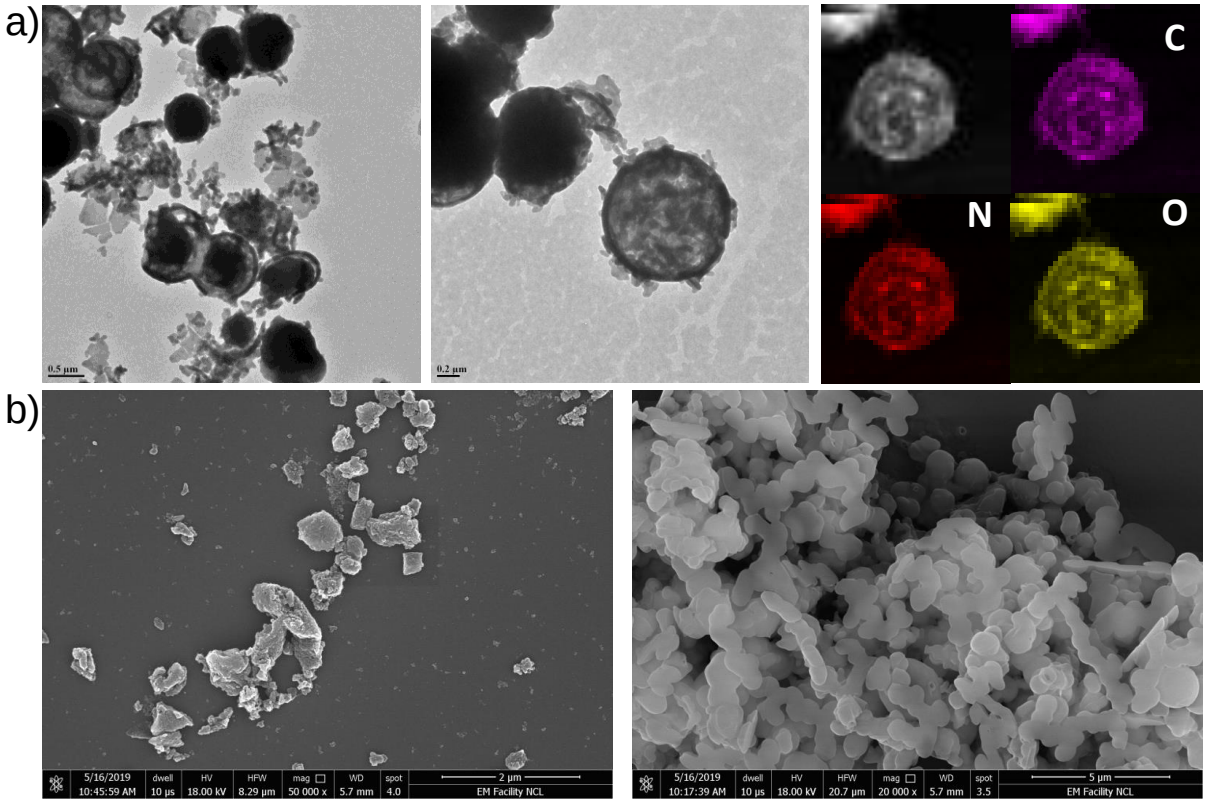

Figure S13: a) TEM images and corresponding elemental mapping, and b) FE-SEM images of **M1**.

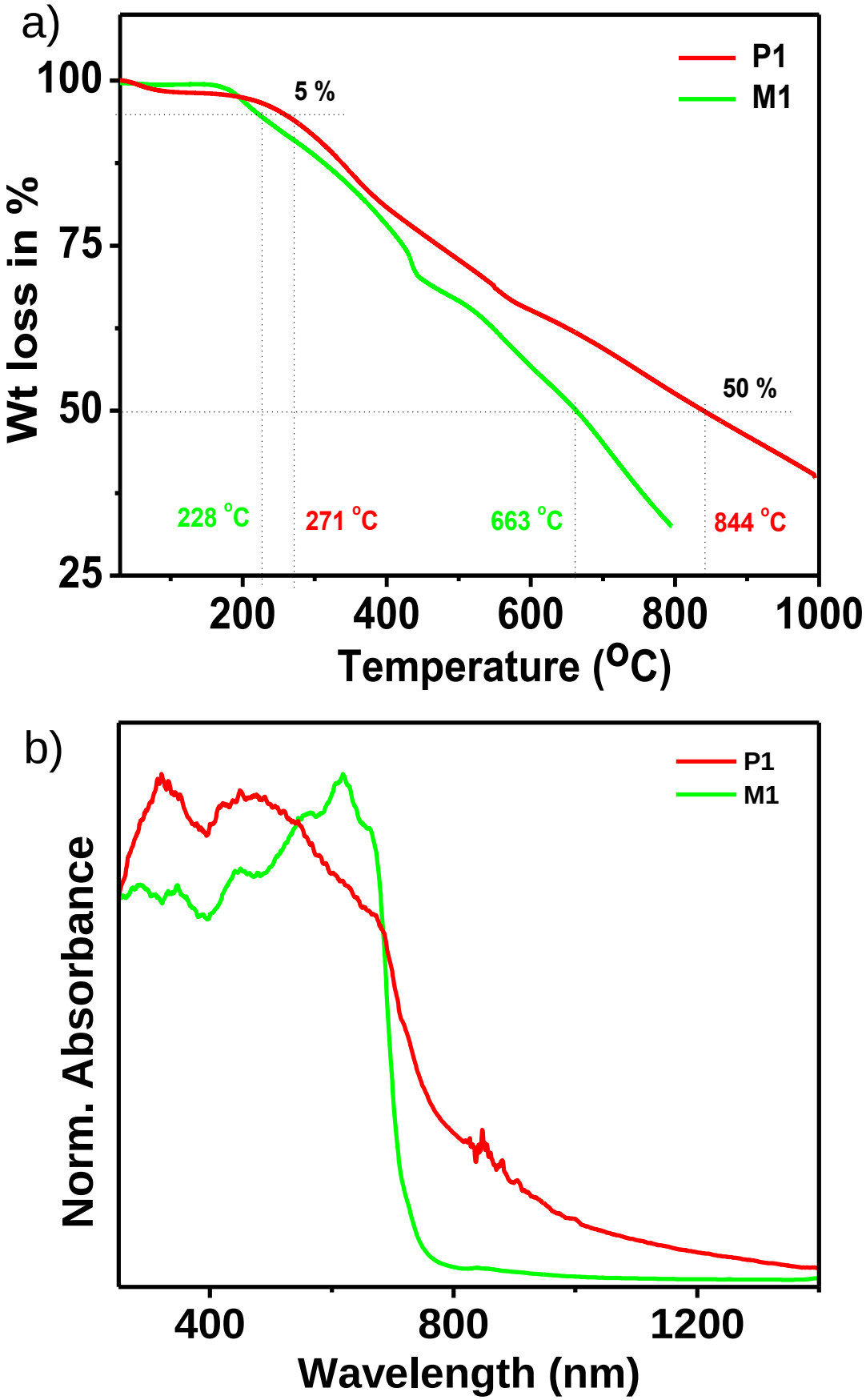

Figure S14: a) Thermogravimetric analysis and b) solid-state absorbance spectra of **M1** and **P1**.

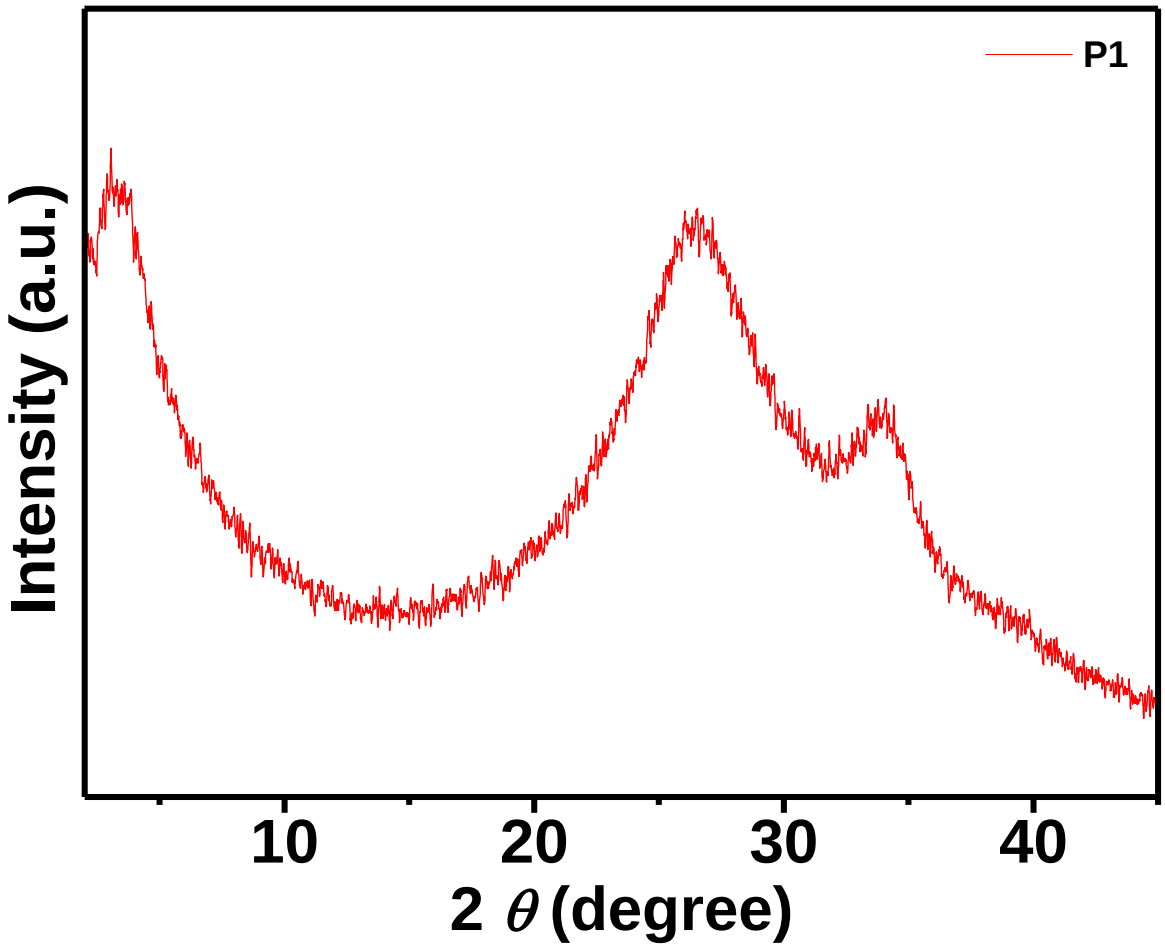

Figure S15: Powder X-ray diffraction pattern of **P1**.

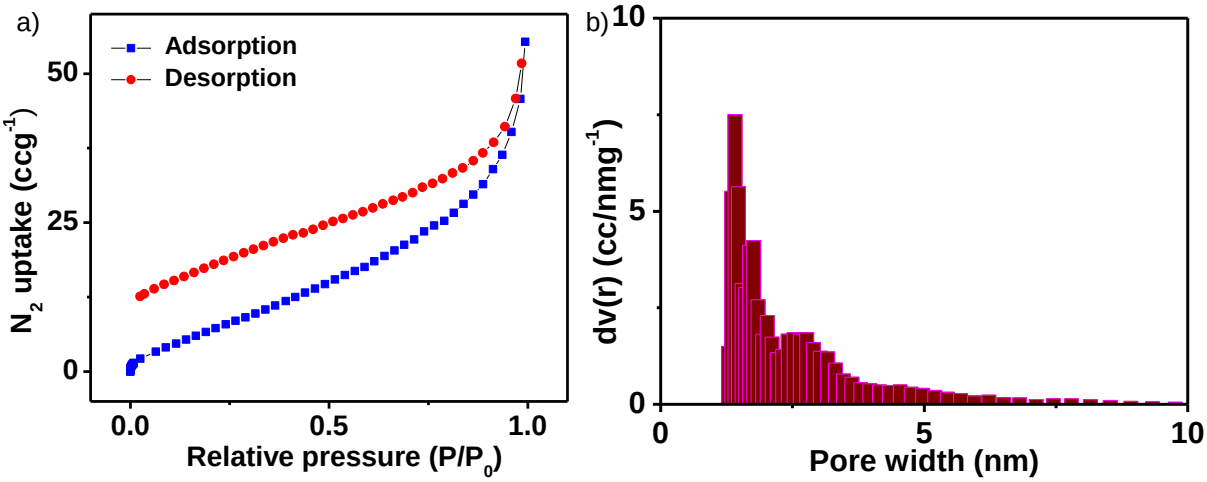

Figure S16: a) Brunauer-Emmett-Teller N_2 sorption isotherm and b) pore-size distribution profile of **P1**.

Electrochemical Measurements

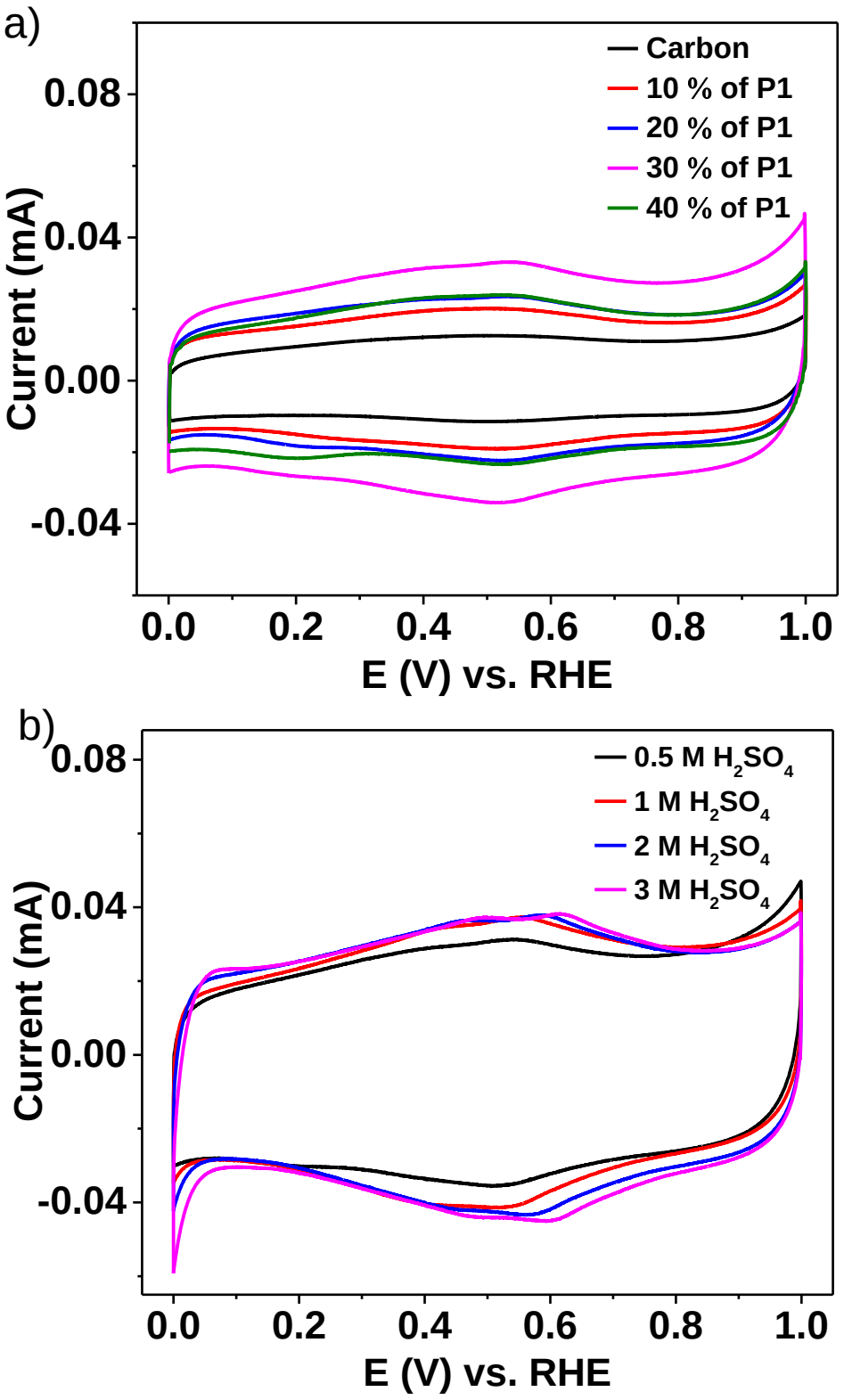

Figure S17: Cyclic voltammetry of **P1** with optimization of a) active material percentage and b) electrolyte concentration in a three-electrode cell.

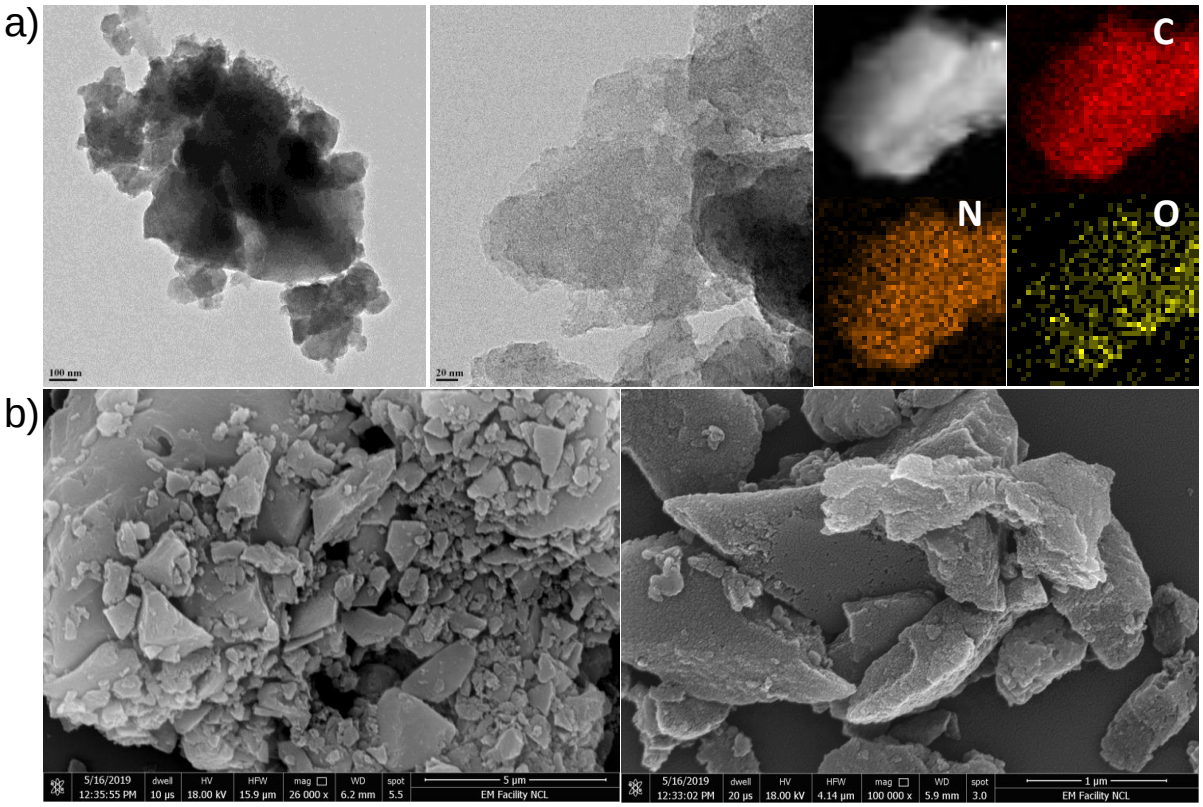

Figure S18: a) TEM images and corresponding elemental mapping, and b) FE-SEM images of **P1** mixed with carbon.

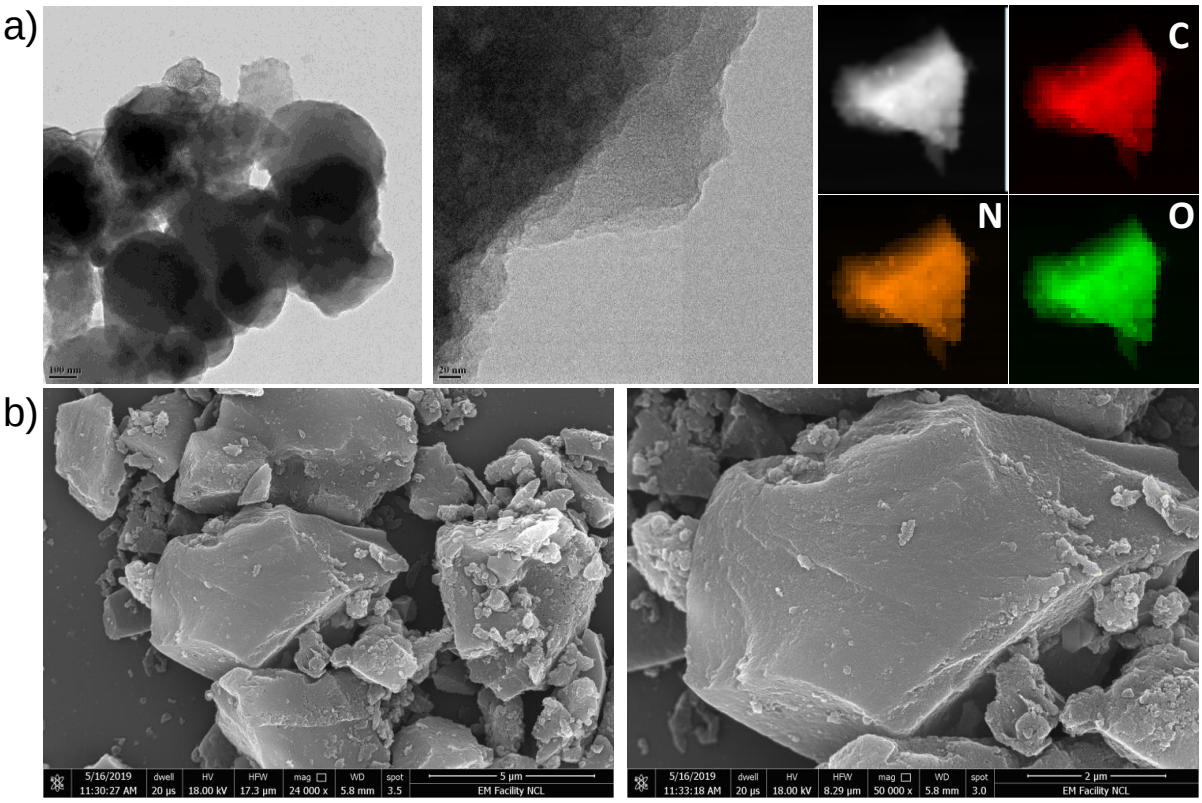

Figure S19: a) TEM images and corresponding elemental mapping, and b) FE-SEM images of **M1** mixed with carbon.

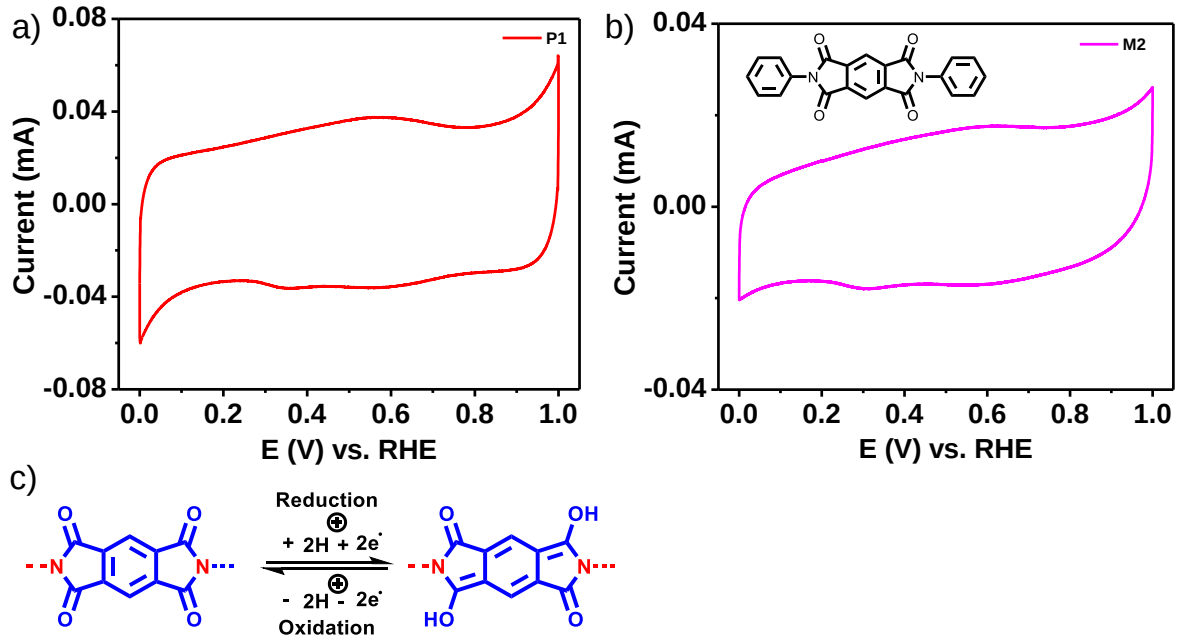

Figure S20: Comparison of CV curve of a) **P1** and b) **M2** at 5 mV s^{-1} scan rate (Inset: chemical structure of **M2**). c) The possible redox behavior of the pyromellitic diimide unit.

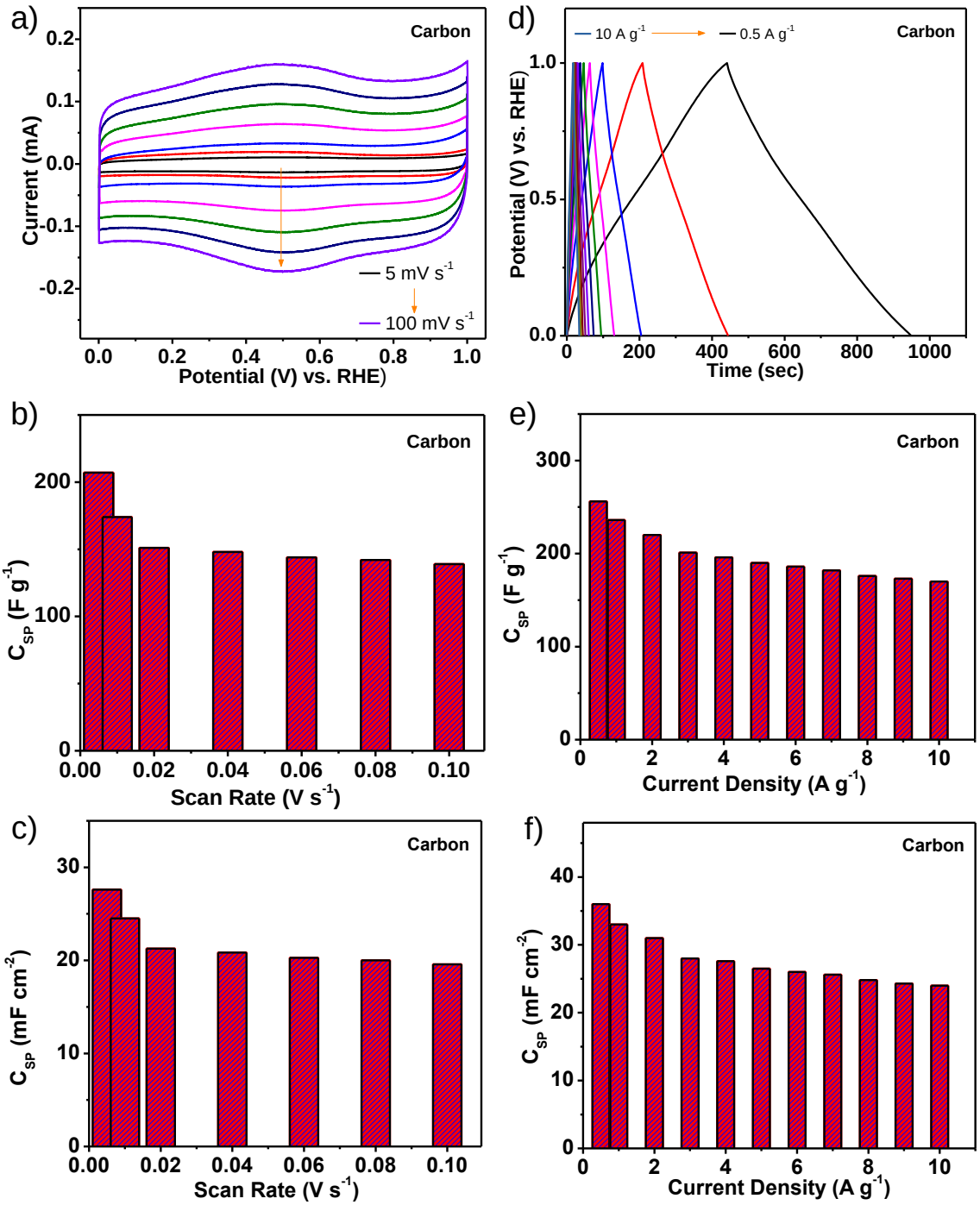

Figure S21: a) CV curves of carbon with increasing scan rate from 5 to 100 mV s^{-1}. b) Specific capacitance c) areal capacitance calculated from the CV of carbon, obtained at different scan rates. d) GCD curves with different current density from 0.5 to 10 A g^{-1} of carbon. e) Specific capacitance f) areal capacitance calculated from GCD of carbon, obtained at different current density.

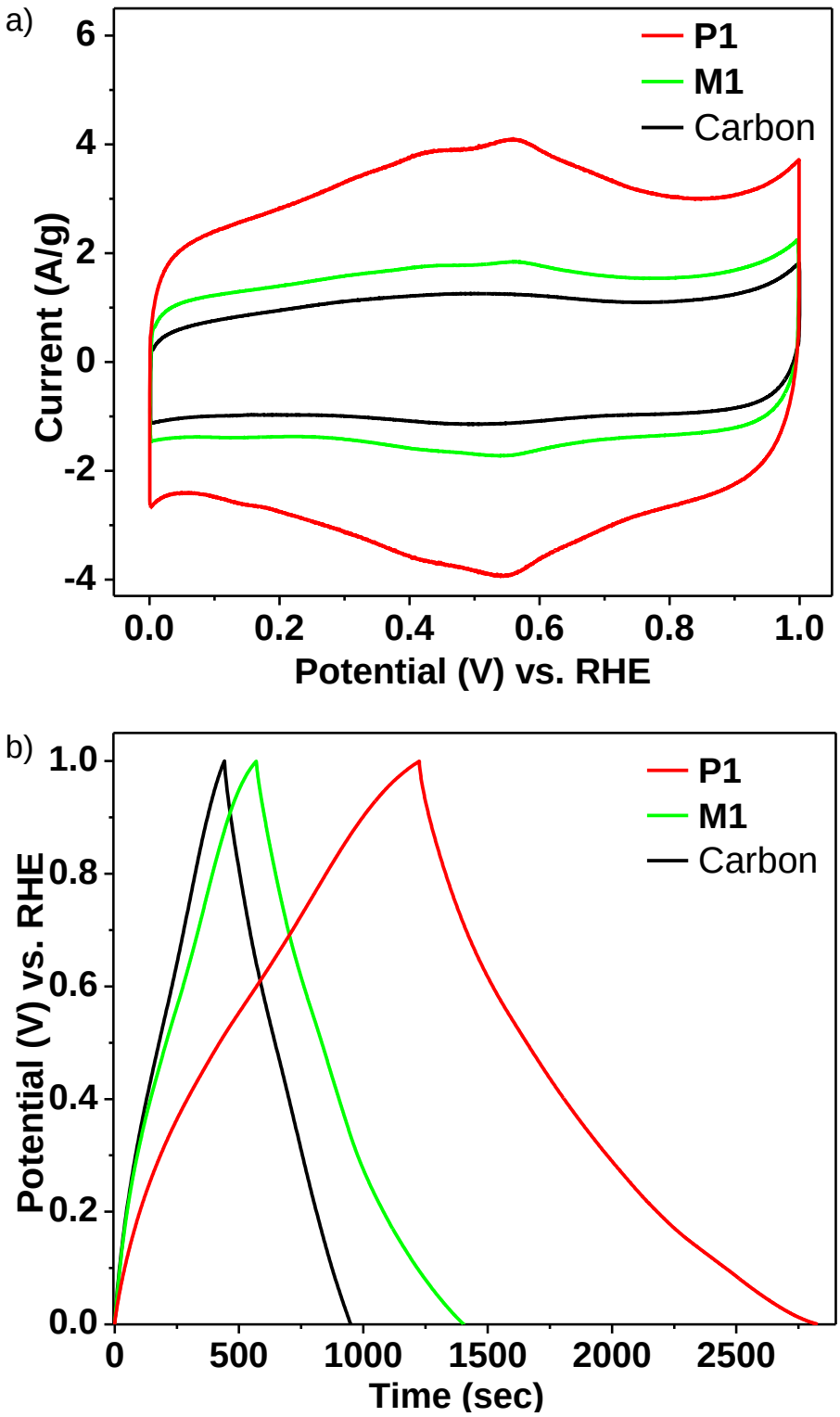

Figure S22: Comparison of a) CV and b) GCD curves at current densities of 0.5 A g^{-1} of carbon, **M1**, and **P1**.

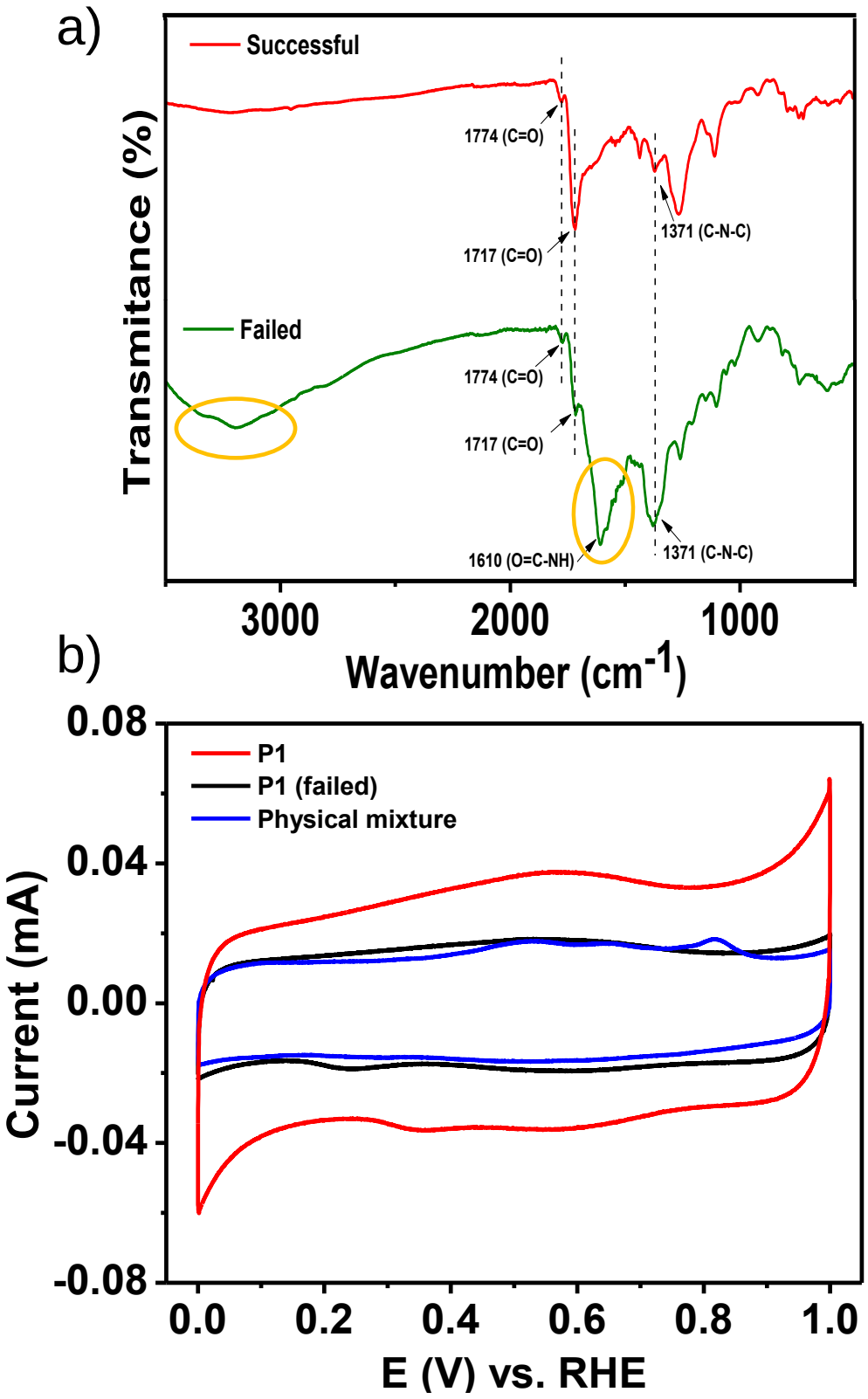

Figure S23: a) Comparison of FTIR of successful and failed polymer **P1** and b) Comparison of CV curves of **P1**, **P1 (failed)** and, **physical mixture of monomers** at 5 mV s^{-1} scan rate. *The unsuccessful **P1** sample was prepared by refluxing the monomers for 12 hours and quenched with water to get precipitate.*

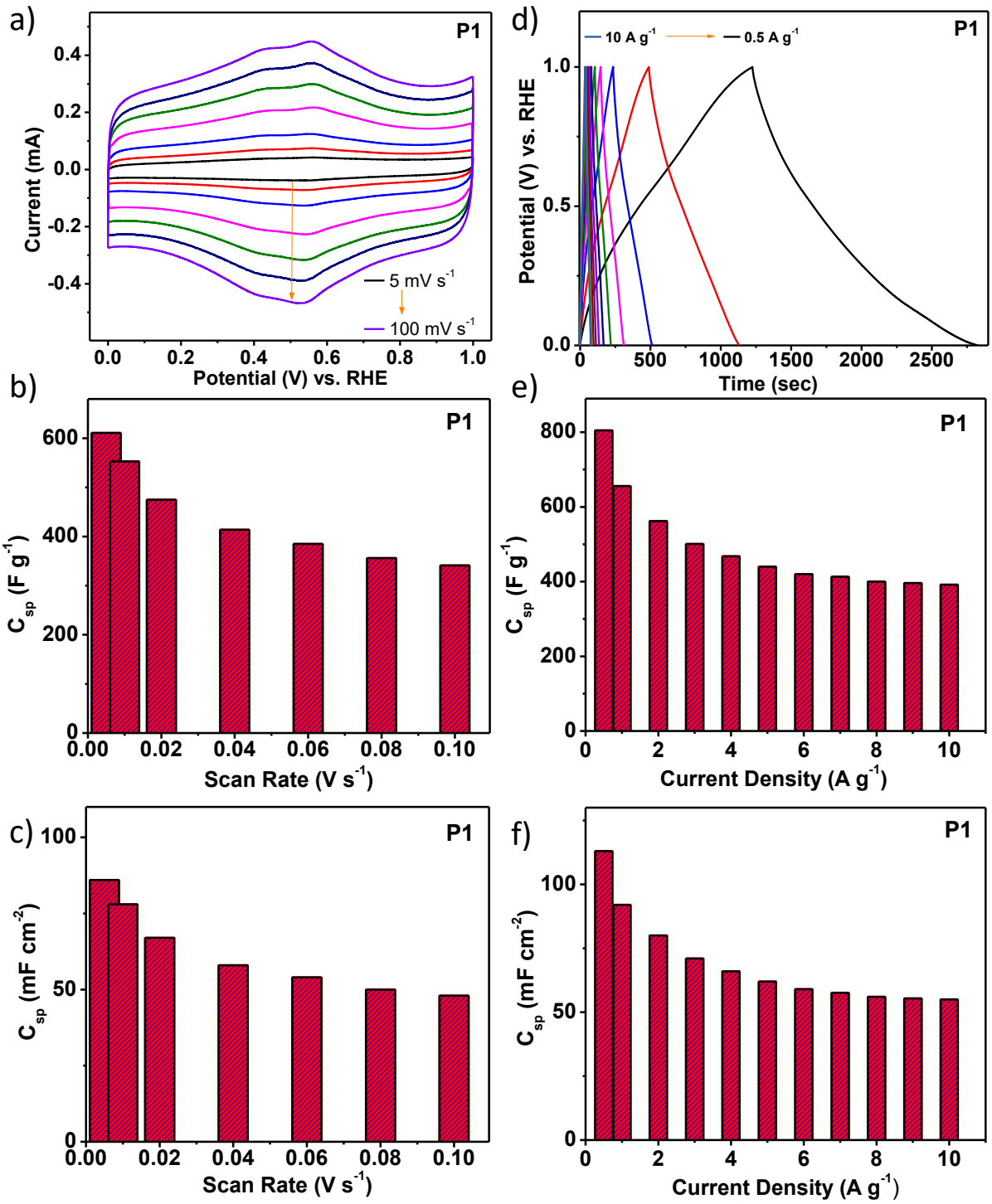

Figure S24: a) CV curves of **P1** with increasing scan rate from 5 to 100 mV s^{-1}. b) Specific capacitance c) areal capacitance calculated from the CV of **P1**, obtained at different scan rates. d) GCD curves with different current density from 0.5 to 10 A g^{-1} of **P1**. e) Specific capacitance f) areal capacitance calculated from GCD of **P1**, obtained at different current density.

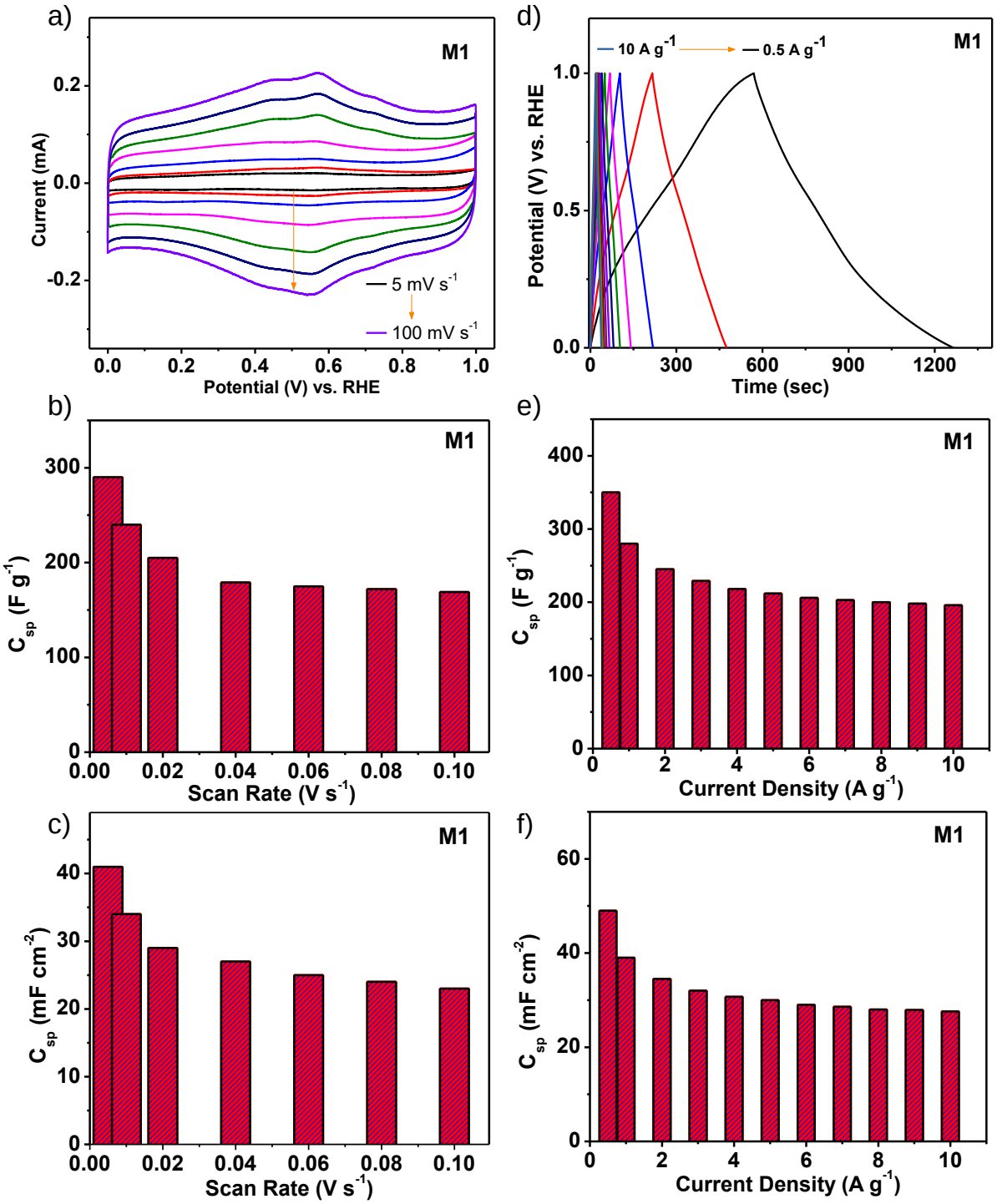

Figure S25: a) CV curves of **M1** with increasing scan rate from 5 to 100 mV s^{-1}. b) Specific capacitance c) areal capacitance calculated from the CV of **M1**, obtained at different scan rates. d) GCD curves with different current density from 0.5 to 10 A g^{-1} of **M1**. e) Specific capacitance f) areal capacitance calculated from GCD of **M1**, obtained at different current density.

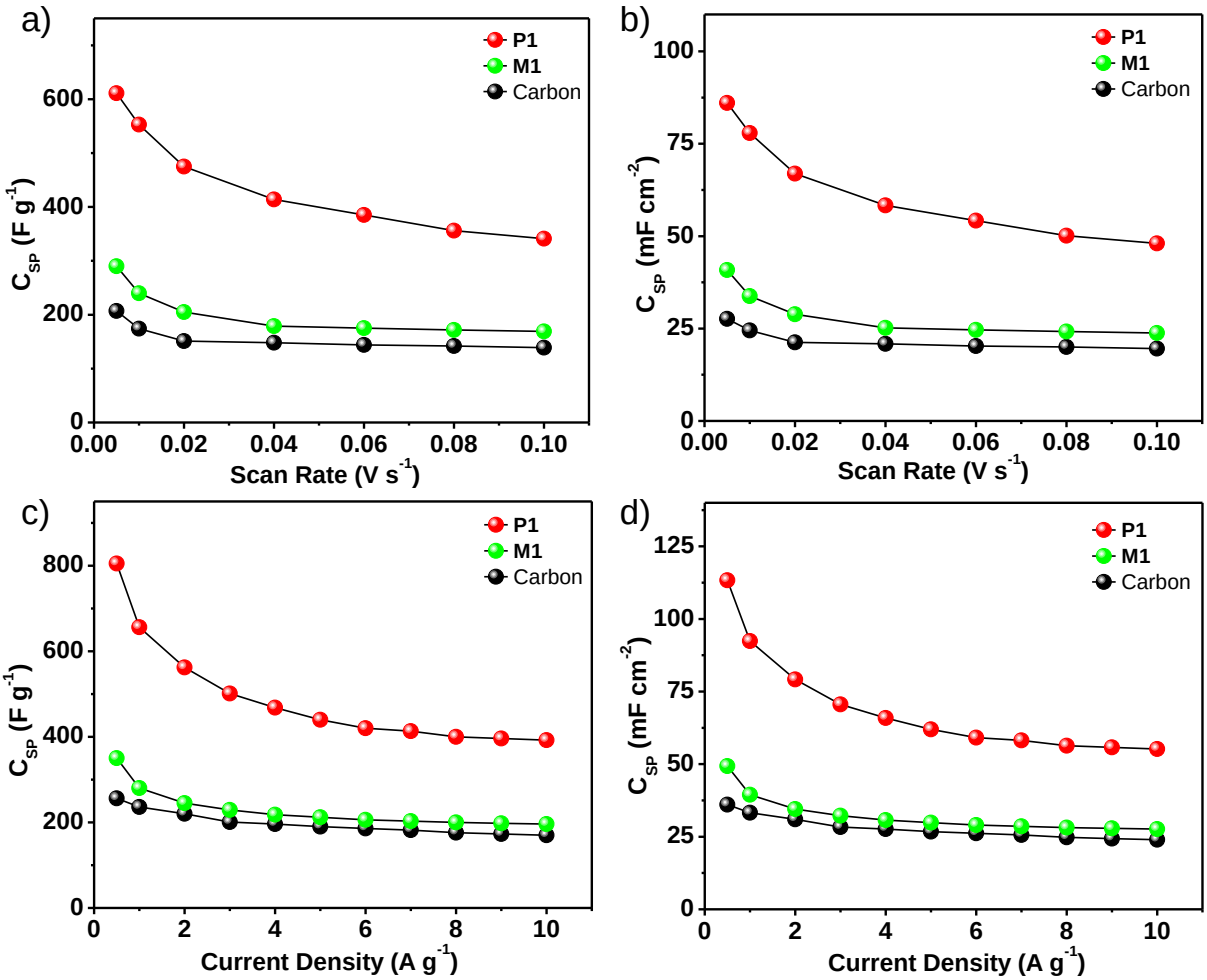

Figure S26: Comparison of a) specific capacitance and b) areal capacitance calculated from the CV of **P1**, **M1,** and carbon, obtained at different scan rates. Comparison of c) Specific capacitance and d) areal capacitance calculated from GCD of **P1**, **M1,** and carbon, obtained at different current densities. (mass loading per electrode area of ~140 µg cm^{-2}).

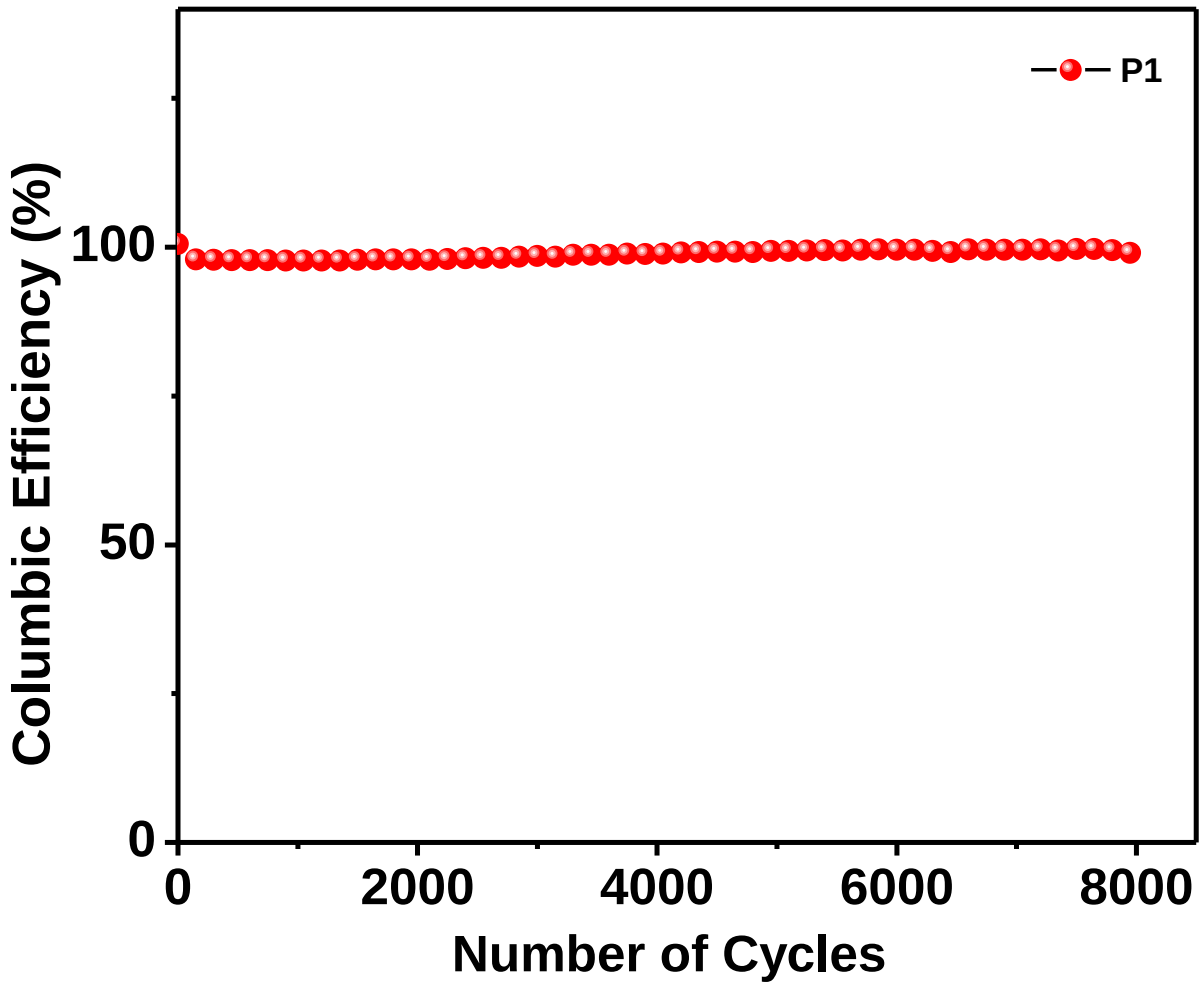

Figure S27: Coulombic efficiency of **P1** up to 8000 GCD cycles.

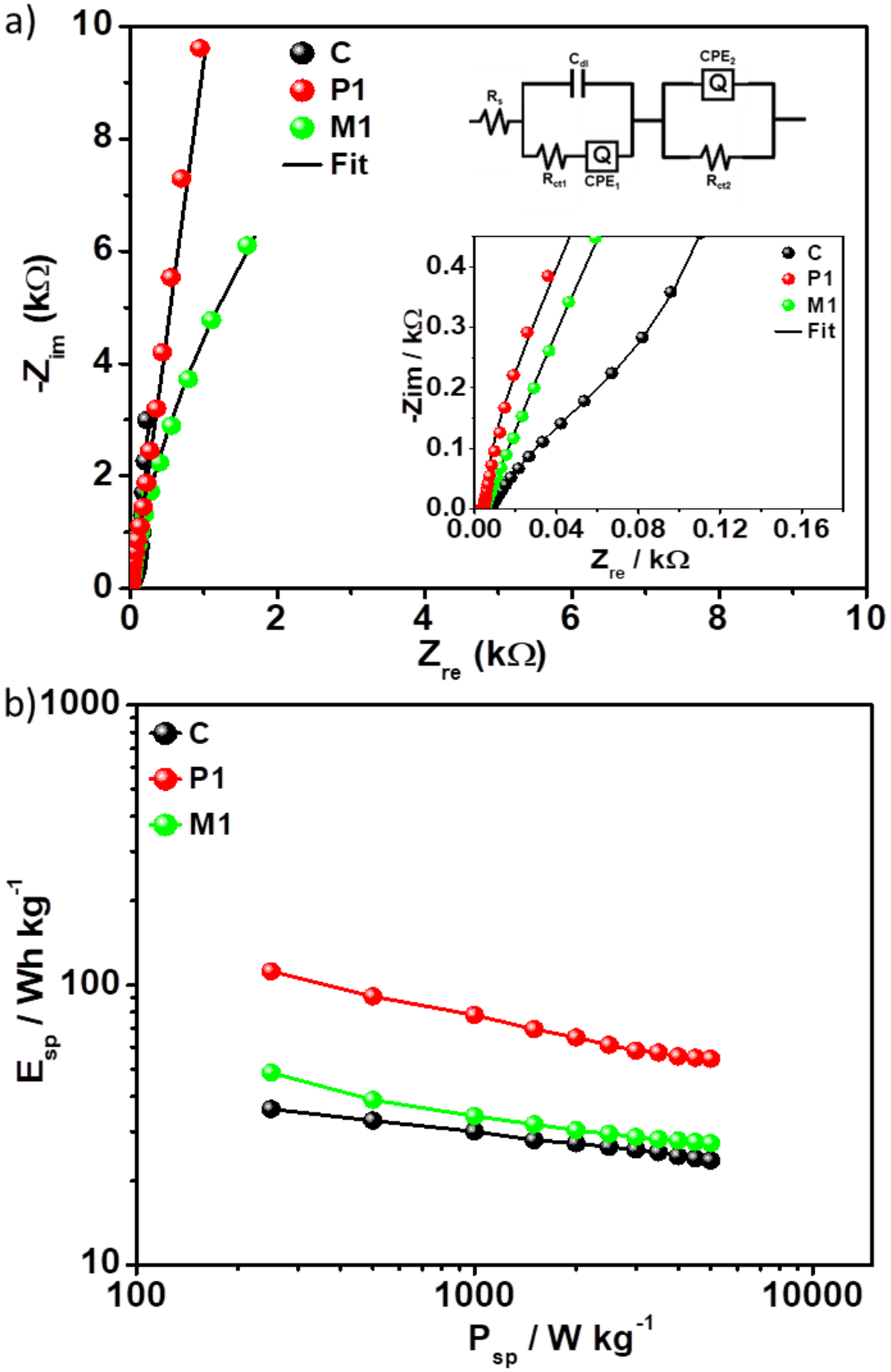

Figure S28: a) Nyquist plot showing the imaginary part versus the real part of the impedance. The inset shows a zoom-in of the high-frequency part and the equivalent circuit diagram. b) Ragone Plot for **P1**, **M1** and carbon.

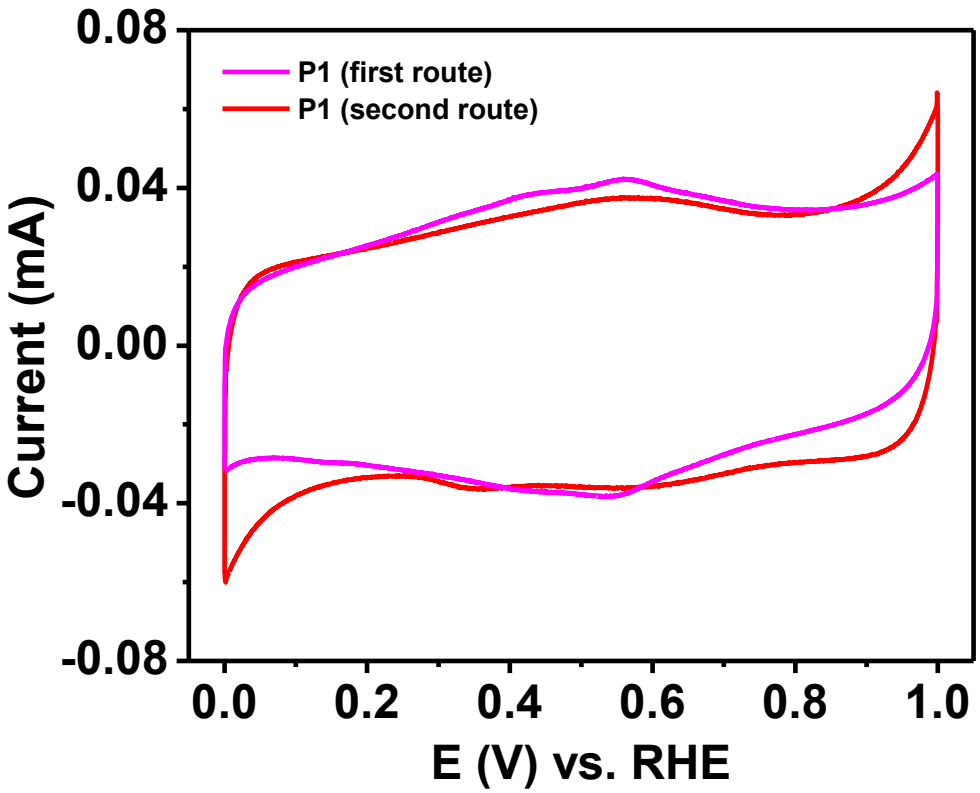

Figure S29: Comparison of CV curves of **P1** synthesized by two different routes at 5 mV s^{-1} scan rate.

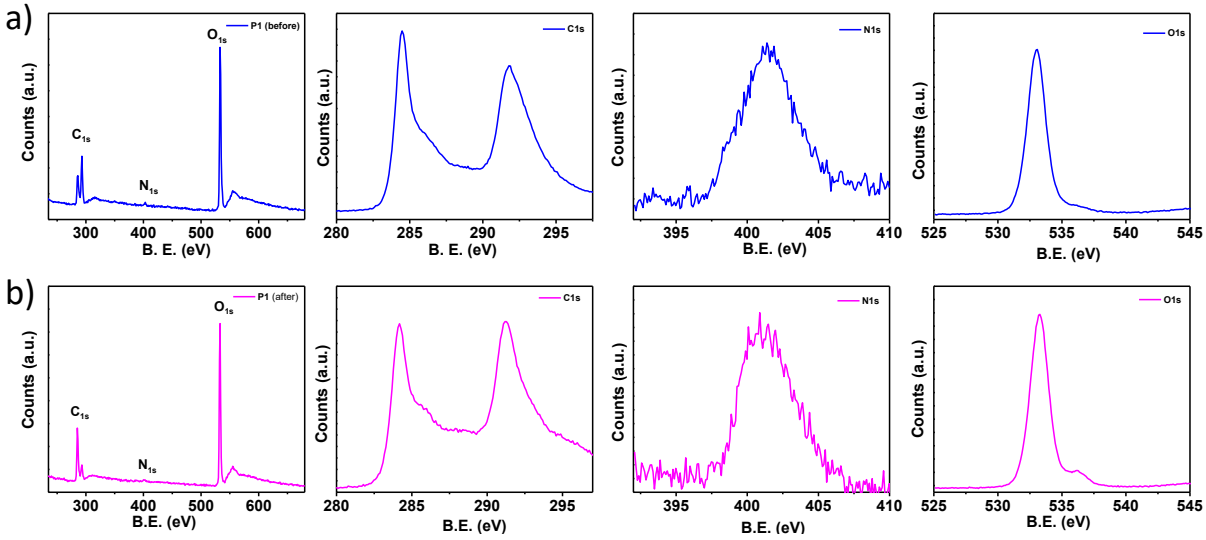

Figure S30: XPS survey scan of **P1** a) before and b) after the electrochemical experiment.

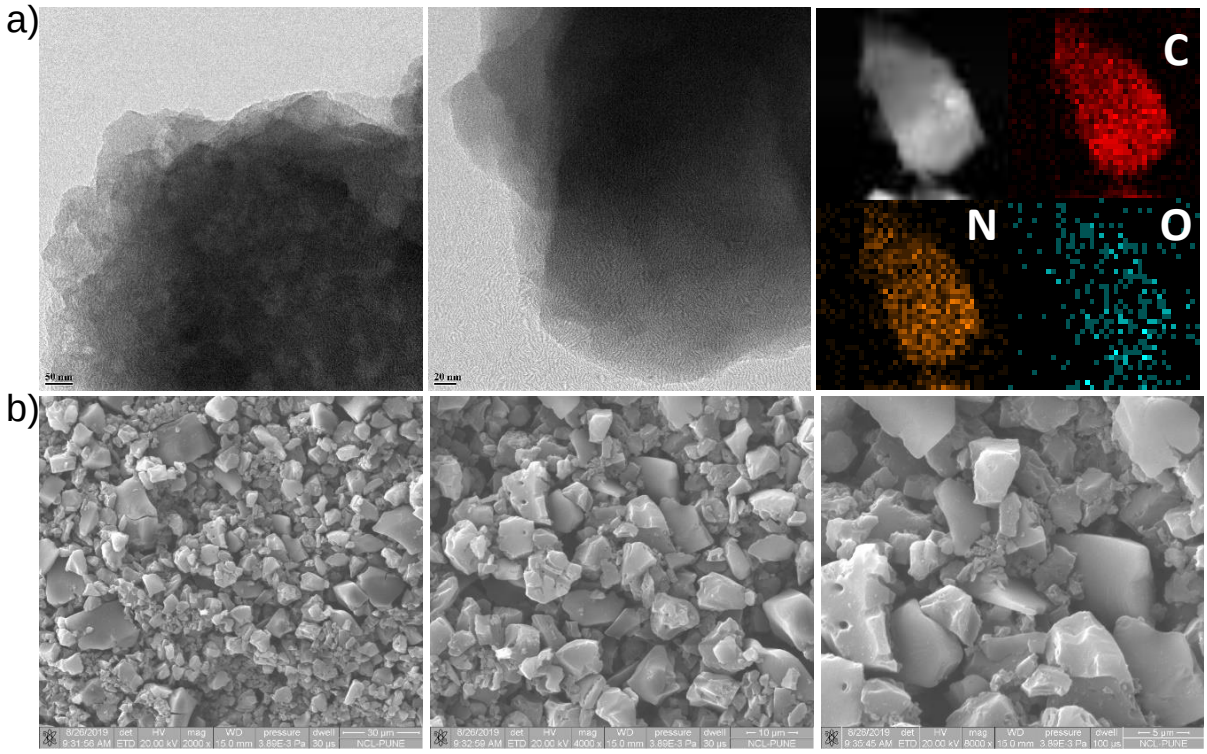

Figure S31: a) TEM images and corresponding elemental mapping of composite **P1** after electrochemical experiment b) SEM images of composite **P1** after the electrochemical experiment.

Tables

Table S1. A comparison of the performance of 2D-polymer (metal-free) based supercapacitors in three-electrode cell.

S. No	Material	Gravimetric capacitance ($F g^{-1}$)	Electrolyte used	Scan Rate / Current Density	Cycle	Ratio	Reference
1.	GNS/PANI composites	1046	6 M KOH	1 mV s^{-1}	-	GNS/PANI:CB:PTFE (75:20:5)	*CARBON* 48, **2010**, 487 - 493
2.	GNS/CB	175	6 M KOH	10 mV s^{-1}	6000	GNS/CB (90:10)	*CARBON* 48, **2010**, 1731 - 1737
3.	PAG80	480	2 M H_2SO_4	0.1 A g^{-1}	-	GO/PANI (80:20)	*Chem. Mater.* **2010**, 22, 1392 - 1401
4.	GPCP	233	1 M H_2SO_4	20 mV S^{-1}	1500	-	*ACS Nano*, 3, **2009**, 1745 - 1752
5.	PANI/GO	531	1 M H_2SO_4	200 mA g^{-1}	-	PANI/graphite oxide (100:1)	*Electrochem. Commun.*, 11, **2009** 1158 - 1161
6.	G-PNF_{30}	210	1 M H_2SO_4	0.3 A g^{-1}	800	-	*ACS Nano*, **2010**, 4, 1963 - 1970
7.	DAAQ-TFP/carbon black	48 ± 10	1 M H_2SO_4	10 mV s^{-1}	5000	DAAQ-TFP:CB:PVDF (35:60:5)	*J. Am. Chem. Soc.* **2013**, 135, 16821
8.	TpOMe-DAQ	169	3 M H_2SO_4	0.35 A g^{-1}	100000	-	*J. Am. Chem. Soc.*, **2018**, 140, 10941 - 10945
9.	graphene-based electrode	154.1	$EMIMBF_4$ ionic liquid electrolyte	1 A g^{-1}	-	graphene, mixed with 5 wt % Super-P and 10 wt % PTFE	*Nano Lett.* **2010,** 10, 4863 - 4868
10.	TCNQ-CTF-800	383	1 M KOH	0.2 A g^{-1}	5000	TCNQ-CTFs :acetylene black: PTFE (80:10:10)	*Angew. Chem. Int. Ed.* **2018**, 57, 7992 - 7996
11.	Aza-CMP@350	397	1 M H_2SO_4	5 A g^{-1}	10000	Aza-CMP :acetylene black: PTFE (80:10:10)	*Angew. Chem. Int. Ed.* **2011**, 50, 8753 - 8757
12.	CAP-2	233	2 M KCl	1.0 A g^{-1}	10000	CAP-2:CB:PVDF (80:15:05)	*ACS Nano* **2018**, 12, 852 - 860
13.	TPDA-1	469.4	1 M H_2SO_4	1 mV s^{-1}	1000	-	*ACS Sustainable Chem. Eng.* **2018**, 6, 202 - 209
14.	TPC-1	424	6 M KOH	0.1 A g^{-1}	-	TPC-1:CB: PTFE (80:10:10)	*Adv. Mater.* **2014**, 26, 3081 - 3086
15.	TNN-550	298	1 M H_2SO_4	0.2 A g^{-1}	5000	TNN-550:CB: PTFE (85:10:05)	*Energy Environ. Sci.*, **2012**, 5, 9747 - 9751
16.	PAQs	576	0.5 M H_2SO_4	1 A g^{-1}	6000	PAQ:acetylene carbon :PTFE (80:15:05)	*Adv. Mater.* **2018**, 30, 1705710
17.	TpDAB	335	1 M Na_2SO_4	2 mV s^{-1}	1000	PTFE (10 wt %)	*Chem. Commun.*, **2016**, 52, 7592 - 7595
18.	PYBDA	456	2 M H_2SO_4	0.5 A g^{-1}	15000	PYBDA: acetylene black: PVDF (60:20:20)	*Chem. Commun.*, **2018**, 54, 6796 - 6799

19.	PTCT-C	558	6 M KOH	1.0 A g^{-1}	1000	PTCT-C:CB:PTFE (80:10:10)	*Chem. Mater.* **2017**, 29, 4885 - 4893
20.	TpPa-$(OH)_2$	416	1 M phosphate buffer	0.5 A g^{-1}	10000 (66% remain)	TpPa$(OH)_2$: acetylene black: PVDF (75: 10: 15)	*Chem. Mater.* **2017**, 29, 2074 - 2080
21.	HTCP-700	445	1 M H_2SO_4	1 A g^{-1}	10000	HTCP-700: acetylene black: PVDF (80:10:10)	*Chemistry Select* **2018,** 3, 8483 - 8490
22.	TCOP	278	6 M KOH	1 A g^{-1}	3000	TCOP:CB:PTFE (80:10:10)	*Electrochimica Acta* **2018,** 284, 98 -107
23.	IMPC	258	1 M H_2SO_4	0.5 A g^{-1}	5000	IMPC: Conducting Carbon :Binder(80:15:05)	*Energy Environ. Sci.,* **2014,** 7, 728 - 735
24.	BIBDZ	88.4	1 M H_3PO_4	0.5 A g^{-1}	5000	-	*Eur. Polym. J.*, **2017**, 93, 448 - 457
25.	**P1**	**805**	**1 M H_2SO_4**	**0.5 A** g^{-1}	**8000**	**AM:Conducting Carbon:Binder (30:65:5)**	***This work***

***AM** = Active Material; **CB** = Carbon Black.*

Table S2. A comparison of the performance of **P1** and **M1** supercapacitors from two different batches.

	From CV		From GCD	
	C_{SP} (F g^{-1})	C_{SP} (mF cm^{-2})	C_{SP} (F g^{-1})	C_{SP} (mF cm^{-2})
M1	290	41	350	49
	272	39	337	47.5
P1	611	86	805	113
	601	85	771	109

Table S3. A comparison of the specific capacitance from CV at 5 mV s^{-1} scan rate.

	C_{SP} (F g^{-1})
P1 (first route)	611
P1 (second route)	628
P1 failed	320
M1	350
M2	292
Carbon	256
Physical mixture of monomers	290

References

1. M.J. Frisch, G.W. Trucks, H.B. Schlegel, G.E. Scuseria., M.A. Robb, J.R. Cheeseman, G. Scalmani, V. Barone, B. Mennucci, G.A. Petersson, H. Nakatsuji, M. Caricato, X. Li, H.P. Hratchian, A.F. Izmaylov, J. Bloino, G. Zheng, J.L. Sonnenberg, M. Hada, M. Ehara, K. Toyota, R. Fukuda, J. Hasegawa, M. Ishida, T. Nakajima, Y. Honda, O. Kitao, H. Nakai, T. Vreven, J.A. Montgomery, J.J.E. Peralta, F. Ogliaro, M. Bearpark, J.J. Heyd, E. Brothers, K.N. Kudin, V.N. Staroverov, T. Keith, R. Kobayashi, J. Normand, K. Raghavachari, A. Rendell, J.C. Burant, S.S. Iyengar, J. Tomasi, M. Cossi, N. Rega, J.M. Millam, M. Klene, J.E. Knox, J.B. Cross, V. Bakken, C. Adamo, J. Jaramillo, R. Gomperts, R.E. Stratmann, O. Yazyev, A.J. Austin, R. Cammi, C. Pomelli, J.W. Ochterski, R.L. Martin, K. Morokuma, V.G. Zakrzewski, G.A. Voth, P. Salvador, J.J. Dannenberg, S. Dapprich, A.D. Daniels, O. Farkas, J.B. Foresman, J. V Ortiz, Cioslowski, D.J. and Fox, I. Gaussian Wallingford CT., Gaussian 09, Revis. C.01. (**2010**).
2. F. Glendening, E. D, Reed, A. E, Carpenter, J, E, Weinhold, NBO Version 3.1 (**2003**).
3. K. Momma, F. Izumi, VESTA 3 for three-dimensional visualization of crystal, volumetric and morphology data, *J. Appl. Crystallogr.* **2011**, *44*, 1272-1276.
4. J. Bae, M. K. Song, Y. J. Park, J. M. Kim, M. Liu, Z. L. Wang, Fiber Supercapacitors Made of Nanowire-Fiber Hybrid Structures for Wearable/Flexible Energy Storage, *Angew. Chem. Int. Ed.* **2011**, *50*, 1683-1687.
5. Q. Wanga, X. Wang, J. Xu, X. Ouyang, X. Hou, D. Chen, R. Wang, G. Shen, Flexible coaxial-type fiber supercapacitor based on NiCo2O4 nanosheets electrodes, *Nano Energy*, **2014**, *8*, 44-51.
6. D. Z. Rogers, Improved synthesis of 1,4,5,8,9,12-hexaazatriphenylene, *J. Org. Chem.* **1986**, *51*, 3904-3905.
7. N. Lahiri, N. Lotfizadeh, R. Tsuchikawa, V. V. Deshpande, V. Louie, Hexaaminobenzene as a building block for a Family of 2D Coordination Polymers, *J. Am. Chem. Soc.* **2017**, *139*, 19-22.
8. A. J. McKerrow, M. A. Fox, J. Leu, P. S. Ho, Preparation and characterization of polyimide alternating copolymers incorporating N, N′-bis-(4-anilino)-1,2,4,5-benzene bis(dicarboximide), *J. Polym. Sci. Part A: Polym. Chem.* **1997**, *35*, 319–327.